THESIS FOR THE DEGREE OF LICENTIATE OF TECHNOLOGY

Nonresonant high-frequency actuation of carbon based nanoelectromechanical oscillators

AXEL MARTIN ERIKSSON

Department of Applied Physics
CHALMERS UNIVERSITY OF TECHNOLOGY
Göteborg, Sweden 2015

Nonresonant high-frequency actuation of carbon based nanoelectromechanical oscillators
AXEL MARTIN ERIKSSON

Licentiatuppsats vid Chalmers Tekniska Högskola

Department of Applied Physics
Chalmers University of Technology
SE-412 96 Göteborg
Sweden
Telephone +46–(0)31–7721000

Cover: Carbon based nanoelectromechanical oscillators constituted by an integrated graphene sheet (top), an isolated graphene sheet (center) and a carbon nanotube (bottom).

Typeset in LaTeX. Figures created using Matlab, Mathematica and PowerPoint.

Chalmers Reproservice
Göteborg, Sweden 2015

Nonresonant high-frequency actuation of carbon based nanoelectromechanical oscillators

AXEL MARTIN ERIKSSON
Department of Applied Physics
Chalmers University of Technology

ABSTRACT

Carbon based nanoelectromechanical oscillators outperform their predecessors in many ways. In particular, their extraordinarily high quality factors make them very promising for sensor applications. To operate the nano oscillators, different kinds of actuation mechanisms are utilised, for instance direct or parametric resonance. Nonresonant actuation of the mechanical vibrations can be achieved if the oscillator is integrated in a resonant LC-circuit or an optomechanical cavity resonator. In these nonresonant actuation mechanisms, the external field couples to the resonance properties of the LC-circuit and optomechanical cavity. The resonance frequencies are typically orders of magnitude higher than the frequencies of the mechanical vibrations.

In this thesis, nonresonant actuation of mechanical vibrations by high-frequency electrical fields are investigated analytically in three different nanoelectromechanical oscillators. Firstly, I analyse a graphene oscillator which is integrated in an RC-circuit which lacks the resonance of an LC-circuit. Secondly, an isolated graphene oscillator where the electrodynamics is determined by the internal properties of the graphene sheet is considered. Finally, I analyse a movable single-electron quantum dot in tunnel contact with an electron reservoir.

The simple capacitance, hydrodynamic and tunneling models used to describe the systems demonstrate the possibility to nonresonantly actuate mechanical vibrations by high-frequency electrical fields. The mechanism is due to the time-delayed electromechanical feedback when the system is driven above the characteristic frequency of the electronic subsystem. Further, nonlinear dissipation is investigated as one possible saturation mechanism of the unstable mechanical motion. The actuation of mechanical vibrations of the isolated graphene sheet is particularly interesting. In this system a geometric resonance of the induced charge oscillations and the vibrational modes seems to allow nonresonant selective actuation of several modes, despite the fact that the driving field is homogeneous.

KEYWORDS: nanoelectromechanical oscillators, nonresonant, mechanical vibrations, graphene, selective mode actuation

LIST OF PUBLICATIONS

This thesis consists of an introductory text and the following papers:

I **Nonresonant high frequency excitation of mechanical vibrations in graphene based nanoresonator**
Axel M. Eriksson, Marina V. Voinova and Leonid Y. Gorelik
New Journal of Physics **17** 033016 (2015)

II **Selective nonresonant excitation of vibrational modes in suspended graphene via vibron-plasmon interaction**
Axel M. Eriksson and Leonid Y. Gorelik
Manuscript in preparation for submission to a scientific journal

III **Nonresonant high-frequency excitation of mechanical vibrations in a movable quantum dot**
Axel M. Eriksson
Manuscript in preparation for submission to a scientific journal

Specification of my contribution to the papers

I I contributed with theoretical and numerical calculations as well as with manuscript preparation.

II I contributed with theoretical and numerical calculations as well as with manuscript preparation.

III I performed the theoretical and numerical calculations and wrote the paper.

Contents

Chapter 1

Introduction

Basic research, curiosity and convenient coincidence has led to a huge number of scientific breakthroughs such as the discovery of X-rays and penicillin. All these examples emphasise the importance of not being too determined on solving a specific problem and disregard events that do not seem to lead to the stated goal. On the other hand, theoretical physics is solely speculations without confirming it by experiments. Therefore, theoretical physicists have mainly two tasks. One of them is to investigate theories and propose new experimental studies of the theoretical findings. The other task is to produce mathematically convenient descriptions which can explain existing experimental results. Both theoretical and experimental scientists have to work together in order to overlap the knowledge gap and overcome technical difficulties.

Another important scientific event was the isolation and experimental characterisation of graphene; a sheet of carbon, only one atom thick [1]. It was an interesting breakthrough for two reasons. Earlier theoretical predictions indicated that the two-dimensional material should be unstable due to thermodynamical fluctuations and therefore should not exist. The other reason is that graphene exhibits some extraordinary properties with a vast potential for applications. The excellent prospect of graphene led to the GRAPHENE Flagship Project which aims to bring the new material from the research labs to applications in every day life of the inhabitants of our globe. The following years will likely bring a lot of new fascinating research results related to graphene and we have an interesting future ahead. However, the focus on graphene may not narrow our curiosity and exclude other materials. The richness of today's technology and societal life comes from combining and hybridising different materials and sciences. Our present and future success lies in our ability to use the benefits from diversity and to keep looking for the unexpected.

1.1 Properties of graphene and carbon nanotubes

Graphene is a 2D-material constituted by a single layer of carbon atoms in a honeycomb lattice with extraordinary properties [2, 3]. Graphene has a very high tensile strength and stiffness due to the strong sp^2-hybridised covalent σ-bonds between

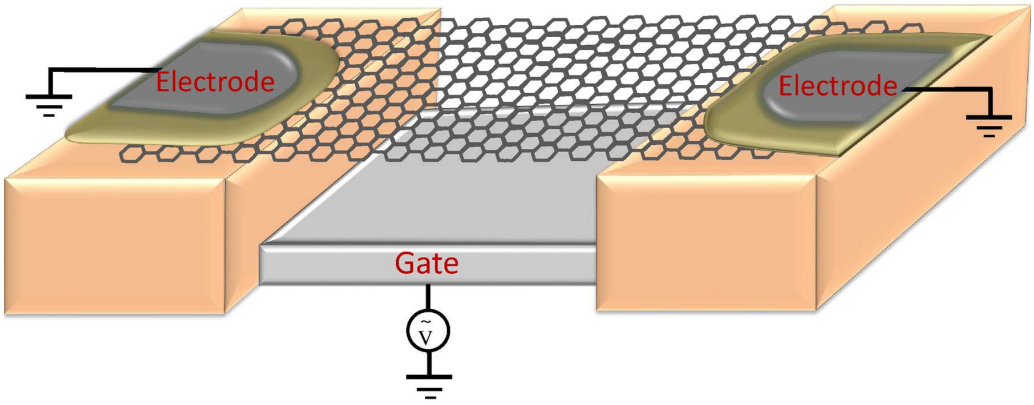

Figure 1.1: A graphene nanoelectromechanical oscillators connected to electrodes. It can be actuated mechanically by applying an ac-gate voltage.

the atoms [4]. However, since graphene is only one atom thick it is very flexible. The electrical properties of graphene can to a good approximation be deduced from the p-orbitals perpendicular to the graphene membrane. Tight-binding calculations for the dispersion of the p-electrons predict linear Dirac cones at each corner of the Brillouin zone.

The properties of graphene can be drastically modified by wrapping it around and forming tubes. These tubes are called carbon nanotubes (CNT) and are typically longer than a micrometer but only a few nm in diameter. CNTs are often referred to as one-dimensional objects because of the strong quantisation of the electronic wave functions around the circumference of the tube. A CNT can be either metallic or semiconducting with a bandgap of ~ 1 eV, depending on the chiral angle and the diameter of the tube. Similar to graphene, CNTs have high tensile strength, stiffness and low mass which make them suitable for nanoelectromechanical oscillator systems.

1.2 Nanoelectromechanical oscillators

Nanoelectromechanical systems are devices which combine mechanical and electronic properties of its constituent parts at the nanoscale. One common set up is to suspend graphene sheets or CNTs over a trench where they can vibrate freely. The clamped parts are connected to electrodes in order to integrate the oscillator into an electrical circuit. The carbon oscillator can then be actuated and tuned by gate electrodes, fig. 1.1.

Applications of nanoelectromechanical oscillators take advantage of the extraordinary material properties as well as the high electromechanical coupling in the systems [5]. The greatest use of carbon based nanoelectromechanical systems will likely be in sensor applications [6]. As a simplified example, if a molecule adsorbs on the movable part of the membrane its vibrational frequency will be slightly shifted. This shift can be read out via the electrodes and thereby be used detect

and measure the mass of the adsorbed particle [7, 8]. Further, the adsorption can affect the electrical properties of the oscillators which gives more information about the particle. The information can be combined to determine what kind of particle was adsorbed. The resulting system is an artificial nose device which could be used to track hazardous gases. Similar systems could also be used to sense charges [9], forces [10] and positions [11] at the nanoscale and be used in electrical filters [12] and transducers [13].

To operate the oscillators, periodic forces of electric or optical origin are utilised to actuate mechanical vibrations. In many cases, the applied force is in resonance with the vibrational mode frequency, [5, 14–16]. However, this thesis focuses on a nonresonant effect. The actuation of a nanomechanical systems is considered to be nonresonant if the actuation mechanism is independent of the relation between the applied driving frequency and the vibrational frequency.

An example of this is the shuttle instability [17, 18] which is the nanoelectromechanical analogue of the Franklin's lightning bell. When a movable conducting particle is situated between two voltage biased electrodes the stationary point of the particle becomes unstable and starts to shuttle charge between the electrodes. Mechanical oscillations of the particle is thereby actuated at its vibrational frequency although the much slower frequency of the bias voltage is far off-resonance.

In optomechanical devices, nonresonant actuation can be achieved by utilising the time-delayed radiation pressure [19, 20]. The detuning of the driving frequency with respect to the optical cavity affects the effective damping of the mechanical oscillator. This phenomenon was demonstrated for graphene resonators where the graphene sheet was both cooled and mechanically actuated by a laser [21].

A similar nonresonant phenomenon in nanostructures is achieved if the role of the optical cavity is replaced with an electrical LC-circuit [22,23]. The resonator can then be driven by applying a frequency close to the relatively high LC-frequency. The mechanical vibrational frequency will not be resolved at the sides of the LC-resonance if the damping rate of the LC-circuit exceeds the vibrational frequency [23]. The mechanical oscillator can in this case be nonresonantly actuated. In the opposite limit the electromechanical coupling could be used for resolved sideband cooling of the mechanical resonator but would then be a resonant phenomenon [24].

1.3 Underlying research questions

The research presented in the papers at the end of this thesis was initiated by the fundamental question; is it possible to actuate mechanical oscillations in nanoelectromechanical structures nonresonantly at high driving frequencies without utilising resonant properties of e.g., an optical cavity or resonant external circuit? Paper I presents such an actuation mechanism for a graphene oscillator integrated as an element of an electrical RC-circuit.

The results triggered the question; is it possible to obtain a similar actuation mechanism utilising the internal electronic properties in an isolated graphene sheet? According to paper II, the answer to this question is yes.

The results of paper I also raised the question; how is the actuation mechanism affected if the quantum nature of electrons are pronounced, which often is the case in nanostructures? In paper III, this question is addressed by investigation of a nanoelectromechanical system represented by a movable single-level quantum dot.

1.4 Thesis Aim and Outline

The aim of this thesis is to provide the background which motivates the work and to prepare readers who are new to the field of nanoelectromechanical oscillators to read the articles. The thesis also serves as a deeper discussion of the physics involved and the limitations and approximations made.

The following three chapters of the thesis describe the analytical models used in the the three papers, respectively. After these chapters, the results of the papers are briefly discussed and compared. Finally, I give an outlook on possible extensions and future work.

Chapter 2

Electromechanical interaction in integrated graphene oscillators

In this and the following chapter I will discuss the models used to describe the electromechanical interaction in the graphene based oscillators considered in papers I and II. I will discuss both the mechanical and the electrical subsystems and the interaction between them which leads to the electromechanical feedback coupling. Under the right conditions, the electromechanical interaction leads to an instability and exponential growth of the mechanical amplitude. This electromechanical instability is the main result of paper I. In a physical system the amplitude growth has to be saturated. One possible candidate for the saturation is nonlinear mechanical dissipation which will be briefly discussed in the final section of this chapter.

2.1 Integrated graphene oscillator system

The model system consists of a doped graphene sheet suspended over a cavity, fig. 2.1. The sheet is free to perform vertical oscillations and is clamped to an insulating substrate. An oxide layer creates a resistive link between the graphene sheet and bulk electrodes, through which electrons can tunnel. Further, a gate electrode is placed below the structure which can adjust the electrical potential on the movable part of the graphene sheet. The graphene membrane can therefore be viewed as an integrated element with the gate and bulk electrodes.

The system exhibits an electromechanical feedback which generates the nonresonant actuation phenomenon. When the gate electrode adjusts the electrical potential on the sheet away from the potential of the bulk leads, a current will flow through the oxide layer and charge the sheet. When the graphene sheet is charged the electrical field from the gate will exert an unbalanced force on the movable part of the sheet and it will deflect. The deflection changes in its turn the electrical potential, and thereby the charge flow to the sheet. By this means there is a feedback on the mechanical motion. Since the charge response is not instantaneous because of the resistive link, the feedback is time-delayed.

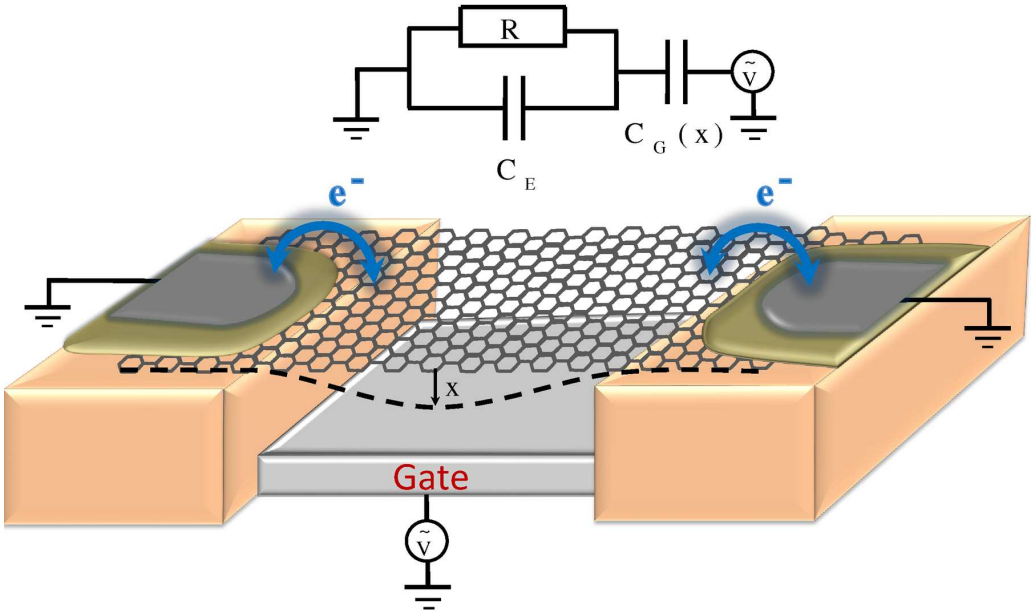

Figure 2.1: Schematic of the suspended graphene membrane oscillator. It is separated from the grounded metallic electrodes by an oxide layer and can perform vertical oscillations in the trench. The back-gate in the trench induces an electrostatical field on the graphene sheet. The equivalent circuit is drawn above the sketch.

The analysis of this time-delayed feedback is limited to high-frequency external driving at the time-scale of the electronic dynamics. The time-scale of the electrodynamics is assumed to be much shorter than the time-scale of mechanical vibrations.

2.2 Electrodynamics - capacitance model

The electrical subsystem of the graphene membrane will be modelled by the equivalent circuit approach. In this approach the dynamics of the electronic subsystem is mapped to an electrical circuit which captures the qualitative features of the original system. This is done by replacing the physical elements of the system with their electrical counter parts such as resistances and capacitances. For instance, the oxide layers is modelled as classical resistances.

The electrical properties of the graphene sheet will be disregarded, except that its a good conductor. This is because the total resistance is assumed to be dominated by the oxide layers. When an electron tunnels onto the graphene membrane it will redistribute to cancel potential differences within the sheet. The time it takes for the charge to redistribute is assumed to be much shorter than the time between tunnelling events.

The ability of the graphene membrane to store the incoming charge is described by its capacitance. There is a capacitive coupling between the membrane and the bulk electrodes C_E as well as the gate electrode C_G. In the simplest model the capacitances only depend on the geometry of the involved parts and the dielectric function

of the medium between them. However, the bandstructure of the materials may affect the actual capacitance. When the graphene membrane is biased by the gate voltage the emptying or filling of higher energy states affects the total free energy per electron and therefore gives contributions to the capacitance, called quantum capacitance. The gate capacitance which depends on spatial deflections can be modelled as the geometrical C_{g} and quantum C_{q} capacitances coupled in series $C_{\mathrm{G}}^{-1} = C_{\mathrm{g}}^{-1} + C_{\mathrm{q}}^{-1}$, where the smallest of them dominates the total capacitance. The quantum capacitance is important in structures where the graphene sheet is separated by thin oxide layers and for very low charge concentrations in the graphene, i.e. close to the Dirac point [25]. In our considerations the graphene membrane is assumed to be doped and suspended at a relatively large distance from the gate electrode and the quantum capacitance will not be taken into account.

A simple model for the geometrical capacitance can then be obtained from Gauss's law by modelling the graphene sheet and the gate electrode as a parallel-plate capacitor $C_{\mathrm{g}} = \varepsilon A/d$ where ε is the permittivity of the medium, A is the area of the suspended graphene part and d is the distance between the suspended sheet and the back-gate. This model assumes the gate electrode and the suspended graphene to be parallel plates and does not take into account the curvature of the graphene sheet when it is deflected.

The equivalent circuit is schematically pictured in fig. 2.1. The capacitors and resistances to the two bulk electrodes have been modelled as a single capacitance C_{E} and resistance R which does not affect the qualitative analysis. The total capacitance of the graphene membrane is then $C = C_{\mathrm{E}} + C_{\mathrm{G}}$.

When the equivalent circuit is formulated the electrodynamics is obtained by standard circuit analysis. Whenever a tunnelling event occurs the total charge q on the membrane immediately divides into one part q_{E} situated at the electrode capacitor and one part q_{G} situated at the gate capacitor

$$q = q_{\mathrm{E}} + q_{\mathrm{G}}. \tag{2.1}$$

Let us denote the potential on the graphene membrane φ and the time-dependent gate voltage $\tilde{V}_{\mathrm{G}}(t) = V_{\mathrm{G}}\cos(\Omega t)$ which gives the relation

$$q_{\mathrm{G}} = -(\tilde{V}_{\mathrm{G}}(t) - \varphi)C_{\mathrm{G}}. \tag{2.2}$$

Similarly, the charge on the electrode capacitor relates to the potential difference between the grounded electrodes and the membrane. When φ is altered a current will flow through the resistance and we have the equation

$$q_{\mathrm{E}} = C_{\mathrm{E}}\varphi = -RC_{\mathrm{E}}\dot{q}. \tag{2.3}$$

We substitute eq. (2.3) and eq. (2.2) in eq. (2.1) to obtain the dynamical equation for the total charge

$$\dot{q} = -\frac{1}{RC}\Big(q + C_{\mathrm{G}}\tilde{V}_{\mathrm{G}}(t)\Big). \tag{2.4}$$

2.3 Mechanical motion of suspended graphene

The mechanical motion of the suspended graphene oscillators will be modelled by continuum elasticity theory. The aim of this section is to reduce the mechanical degree of freedom to the fundamental flexural mode and describe it as a harmonic oscillator under the influence of an external force. I also briefly comment upon nonlinear dynamics in carbon based nanoelectromechanical systems.

Starting from a more general point, the graphene membrane in the suspended part can deflect in two dimensions within the plane of the graphene sheet and one dimension out-of-plane. Due to nonlinear interaction the in-plane and out of plane motion is coupled. This situation was recently analysed including both nonlinear stretching and bending energies in the Föppl-von Kármán equations [26]. The details of the analysis lies outside the scope of this thesis but I will briefly discuss the main assumptions.

To reduce the complexity of the dynamics, two approximations will be made. The first approximation is that the in-plane motion follows the out-of-plane motion adiabatically. This is because the lowest frequencies of the in-plane vibrational modes are typically on a much faster time-scale than the out-of-plane flexural mode frequencies. A slight damping of the in-plane motion will then quickly drive the in-plane displacement into equilibrium with the out-of-plane deflection. The dynamics is then determined by the out-of-plane motion. Further, nonlinear effects can be neglected for sufficiently small deviations from the flat equilibrium position.

The mechanical motion of the vertical deflection $w(x,t)$ is in these approximations described by the differential equation

$$\rho_g \frac{\partial^2 w(x,t)}{\partial t^2} + \kappa \frac{\partial^4 w(x,t)}{\partial x^4} - T_0 \frac{\partial^2 w(x,t)}{\partial x^2} = F(x,t) \tag{2.5}$$

with 2D-mass density of graphene $\rho_g \approx 0.75$ mg/m^2 [27], bending rigidity κ, built-in tension T_0 and external pressure $F(x,t)$. A static external force can tune the vibrational frequency of the membrane by enhancing the tensile stress.

One useful way to describe the motion in linear systems, as the one described by eq. (2.5), is by its independent vibrational modes. These are found by the following procedure. The homogeneous problem $F(x,t) = 0$ can be solved by separation of variables $w(x,t) = a(t)\Phi(x)$ where the time dependent problem is solved by the harmonic function $a(t) = a\exp(i\omega_n t)$. The resulting equation for the spatial function is an eigenvalue problem on the form

$$\frac{\kappa}{\rho_g}\frac{\partial^4 \Phi(x)}{\partial x^4} - \frac{T_0}{\rho_g}\frac{\partial^2 \Phi(x)}{\partial x^2} = \omega_n^2 \Phi(x) \tag{2.6}$$

with eigenfrequencies ω_n. The boundary conditions corresponding to the clamping reduces the ω_n to a discrete set for which solutions to eq. (2.6) exist. It is benefitial to avoid narrow beam oscillators since they exhibit spurious edge modes which enhances the dissipation [28]. These solutions are the orthogonal spatial mode shapes

Φ_n of the vibrational modes. A general vertical deflection can be written as a superposition of all these independent harmonic modes

$$w(x,t) = \sum_{n=0}^{\infty} \zeta_n(t)\Phi_n(x), \tag{2.7}$$

with amplitudes $\zeta_n(t)$ which oscillate with frequencies ω_n.

Eq. (2.6) can be simplified by the membrane approximation in which the bending regidity is neglected. The membrane approximation is valid in most experimental situations. This is because graphene oscillators are often under the influence of a built-in tensile stress T_0 corresponding to a 1% tensile strain of the graphene sheet [28]. Under this condition, the ratio between the bending and stretching energies are small due to low bending rigidity of graphene $\kappa \approx 1.5$ eV [27].

Finally, the mechanical vibrations of the oscillator are assumed to be fully characterised by the fundamental flexural mode $\Phi_0(x)$ and its amplitude $\zeta_0(t)$. Although other modes might be excited as well, they will only couple weakly to the driving field due to the mismatch between the spatial profiles of the higher vibrational modes and the instantaneously redistributed charge on the membrane. The mechanical motion can therefore be modelled as a single mode driven harmonic oscillator.

2.3.1 Harmonic oscillator

The harmonic oscillator is probably one of the most well known mathematical systems used to model physical features in nature. The reason for this is both that it can be solved exactly and that it has wide applicability. The dynamics in the vicinity of an equilibrium point of a one dimensional system is well approximated by a harmonic oscillator. The only exceptions are strictly nonlinear situations where the quadratic term in the expansion of the potential about the equilibrium point vanishes identically.

2.3.2 Anharmonic oscillator

If the oscillator is actuated to larger amplitudes away from the equilibrium point, nonlinear dynamics cannot be neglected and the motion will be anharmonic. One of the most common models for nonlinear systems is the Duffing oscillator

$$\ddot{x} + \frac{\omega_{\mathrm{m}}}{Q}\dot{x} + \omega_{\mathrm{m}}^2 x + \delta\frac{x}{l} + \eta\left(\frac{x}{l}\right)^2 x = \frac{F}{m}, \tag{2.8}$$

where the nonlinearity becomes important at deflections of the order of l. The nonlinear Föppl-von Kármán equations have no independent stationary solutions on the form as in eq. (2.7). Instead the dynamics can be described by coupled Duffing oscillators exhibiting mode coupling [26]. For a deeper discussion of nonlinear effects in oscillating systems the reader is encouraged to look into reference [29].

The origin of the nonlinear terms can be intrinsic such as the geometrical nonlinearity in suspended graphene oscillators. However, nonlinear terms of this kind

will not be included in the models used in any of the papers since they do not qualitatively affect the phenomenon of interest. Another source of nonlinear dynamics arise from nonlinear external forces. This is a type of nonlinearity which will show up in the electromechanical coupling presented below. However, only the response to the linearised equations will be analysed.

2.4 Coupled electromechanical motion

If the mechanical and electrical subsystems do not interact their dynamics can be treated independently. The interesting physics, and one great advantage of nano-electromechanical systems, comes from the interaction between the two degrees of freedom.

The charge dynamics described by eq. (2.4) is coupled to the mechanical subsystem since the gate capacitance changes with the vertical deflection x of the membrane. A more precise formulation of the charge dynamics is therefore

$$\dot{q} = -\frac{1}{RC(x)}\Big(q + C_{\mathrm{G}}(x)\tilde{V}_{\mathrm{G}}(t)\Big). \tag{2.9}$$

which is a nonlinear equation in x. Let us assume the deflections to be small $x/d \ll 1$ and expand the parallel-plate gate capacitance $C_{\mathrm{G}}(x) = \varepsilon_0 A/(d-x) \approx C_{\mathrm{G}}(0)(1 + x/d + (x/d)^2)$. For convenience the equations are scaled to dimensionless time $\tau = t/(RC(0))$, charge $Q = q/(V_{\mathrm{G}}C_{\mathrm{G}}(0))$, driving frequency $\tilde{\Omega} = RC(0)\Omega$, deflection $X = x/d$ and damping $\tilde{\gamma} = RC(0)\gamma$. The linearised version of eq. (2.9) about $X = 0$ becomes

$$Q_\tau \approx -Q - \cos(\tilde{\Omega}\tau) + \Big(\eta Q - (1-\eta)\cos(\tilde{\Omega}\tau)\Big)X, \tag{2.10}$$

with capacitance ratio of the gate capacitance $\eta = C_{\mathrm{G}}(0)/C(0)$ and derivative notation $Q_\tau = \partial Q/\partial\tau$. This equation describes the influence of the mechanical deflection on the charge dynamics.

On the other hand, the mechanical motion of the membrane will be affected by the charge on the movable part. When the freely vibrating part of the graphene is charged the electrical field from the gate exerts a force on the charges. The force can be obtained by differentiating the stored energy with respect to x while keeping the electrical potentials constant [30]

$$X_{\tau\tau} + \frac{\tilde{\omega}_{\mathrm{m}}}{Q}X_\tau + \tilde{\omega}_{\mathrm{m}}^2 X = \frac{1}{2m}\frac{\partial C_{\mathrm{G}}(x)}{\partial x}\left(\varphi - \tilde{V}_{\mathrm{G}}(t)\right)^2. \tag{2.11}$$

Since $\varphi = (C_{\mathrm{G}}(x)\tilde{V}_{\mathrm{G}}(t) + q)/C(x)$ depends on q the mechanical motion is coupled to the charge dynamics.

2.5 Instability of mechanical motion

The electromechanical coupling presented in eqs. (2.10) and (2.11) exhibits rich dynamics also when linearised with respect to X. In this section, I will present three

different instability mechanisms exhibited by this coupling which can be utilised to actuate mechanical oscillations. Two of the mechanisms are direct resonance and parametric instability which are very well known resonant phenomena. The third is the nonresonant phenomenon which is the main focus of this thesis. To analyse these mechanisms let us assume the applied field to be small $\varepsilon = C_{\mathrm{G}}(0)V_{\mathrm{G}}^2/md^2\omega_{\mathrm{m}}\nu_{RC(0)} \ll 1$, with $\nu_{RC(0)} = 1/(RC(0))$.

2.5.1 Resonant instability mechanisms

To see the resonant phenomena the analysis can be simplified by the following approximation: In most applications and experimental situations, the mechanical vibration is typically on a much slower time-scale than the electrodynamics, in this case $\omega_{\mathrm{m}} \ll \nu_{RC(0)}$. If a driving field with frequency $\Omega \sim \omega_{\mathrm{m}}$ is applied, the fast electronic dynamics will relax quickly to its stationary state where $\dot{q} = 0$. At every point in time $q \approx -C_{\mathrm{G}}(x)\tilde{V}_{\mathrm{G}}(t)$ and the potential on the sheet $\varphi = 0$. This means that the feedback on the mechanical motion via the electrodynamics is neglected. Taking $\varphi = 0$ in eq. (2.11) and linearising with respect to X reduces the mechanical motion to

$$\ddot{X} + \gamma\dot{X} + \omega_{\mathrm{m}}^2 X = \frac{C_{\mathrm{G}}(0)V_{\mathrm{G}}^2}{4md^2}(1+2X)(1+\cos(2\Omega t)), \tag{2.12}$$

which is a forced damped oscillator. Due to the linearity of eq. (2.12) the force terms can be considered independently. The interesting forces are those varying in time since they can pump energy into the system. The force term proportional to $\cos(2\Omega t)$ gives direct resonance [31] while $X\cos(2\Omega t)$ leads to parametric resonance [31]. These actuation mechanisms are briefly described in Appendix A and B.

2.5.2 Nonresonant instability mechanism

The third instability is a nonresonant phenomenon meaning that the condition for the instability is independent of the relation between the driving frequency Ω and the mechanical frequency ω_{m}. The nonresonant instability is an effect which relies on a time-delayed feedback mechanism, in contrast to the resonant phenomena studied above. The instability is obtained when the driving frequency is comparable to the characteristic time-scale of the electrodynamics and can be seen as a consequence of the time-delay in the electronic subsystem. To analyse the nonresonant instability the adiabatic approximation of the electrodynamics has to be relaxed since it assumes instantaneous response.

An integral expression for the charge can be obtained from eq. (2.10) by dividing the charge into two parts $Q = Q_0 + Q_1$. The zeroth-order part Q_0 solves the problem when $X \equiv 0$. It takes the value $Q_0 = -\frac{\cos(\tilde{\Omega}\tau - \vartheta)}{\sqrt{1+\tilde{\Omega}^2}}$, where $\tan(\vartheta) = \tilde{\Omega}$. The correction

Q_1 takes into account the linear term in X and becomes

$$Q_1 = -\int_{-\infty}^{0} d\tau' e^{\tau'} \left[\eta \frac{\cos\left(\tilde{\Omega}(\tau'+\tau) - \vartheta\right)}{\sqrt{1+\tilde{\Omega}^2}} + (1-\eta)\cos\left(\tilde{\Omega}(\tau'+\tau)\right) \right] X(\tau'+\tau). \tag{2.13}$$

Both charge components oscillate at the time-scale of the applied electrical field. Inserting this expression for Q in eq. (2.11) and linearising with respect to X gives the qualitative structure

$$X_{\tau\tau} + \frac{\tilde{\omega}_\mathrm{m}}{Q} X_\tau + \tilde{\omega}_\mathrm{m}^2 X = \mathcal{K}_1 + \mathcal{K}_2 X + \mathcal{K}_3 \cos(2\tilde{\Omega}\tau) + \mathcal{K}_4 X \cos(2\tilde{\Omega}\tau) + \mathcal{K}_5 \cos(\tilde{\Omega}\tau) Q_2, \tag{2.14}$$

where all coefficients $\mathcal{K}_i$ are proportional to the small parameter ε. The static term $\mathcal{K}_1$ adjusts the equilibrium position of the oscillator from 0 to $X_\mathrm{eq} = \mathcal{K}_1/\tilde{\omega}_\mathrm{m}^2$. The second term renormalises the frequency of the mechanical oscillator $\tilde{\omega}_\mathrm{m}^2 \to \tilde{\omega}_\mathrm{m}^2 - \mathcal{K}_2$. The direct and parametric terms $\mathcal{K}_3$ and $\mathcal{K}_4$ are far off-resonance $\omega_\mathrm{m}/\Omega \ll 1$ and will therefore be disregarded. The term $\mathcal{K}_5$ is the interesting one giving rise to the nonresonant instability mechanism.

The term $\mathcal{K}_5$ comes from the applied field acting on the time-delayed charge response Q_1. The rapidly oscillating external field mixes with rapid oscillations of Q_1. The result is slowly oscillating terms at the time-scale of X which carries the electromechanical feedback. The rapidly oscillating terms can be disregarded since they are far off-resonance [31]. For the sake of clarity, we will disregard the trivial static and renormalising terms since they will not change the qualitative result.

In that case, the resulting equation takes the form

$$X_{\tau\tau} + \tilde{\gamma} X_\tau + \tilde{\omega}_\mathrm{m}^2 X = \mathcal{K} \int_{-\infty}^{0} \mathrm{d}\tau'\, e^{\tau'} \cos(\tilde{\Omega}\tau') X(\tau+\tau'), \tag{2.15}$$

$$\mathcal{K} = \eta \frac{1 + (1-\eta)^2 \tilde{\Omega}^2}{1+\tilde{\Omega}^2} \frac{C_G(0)\left(RC(0)V_G\right)^2}{2md^2} \tag{2.16}$$

where X is a function varying slowly in comparison with $\cos(\tilde{\Omega}\tau)$ and $\tilde{\Omega} \sim 1$. To analyse the stability of X we adopt the Ansatz $X = \exp(\lambda\tau)$, with complex frequency λ which has to satisfy the dispersion equation

$$\lambda^2 + \tilde{\gamma}\lambda + \tilde{\omega}_\mathrm{m}^2 = \mathcal{K} \frac{1+\lambda}{(1+\lambda)^2 + \tilde{\Omega}^2}. \tag{2.17}$$

This is a fourth order equation which describes the coupling between the mechanical and electronic subsystems. According to the assumptions made this far, the restrictions $1 \sim \tilde{\Omega} \gg \tilde{\omega}_\mathrm{m} \gg \tilde{\gamma} \sim \mathcal{K}$ apply. To zeroth order in the small parameter $\mathcal{K}$ the complex frequency $\lambda_0 = \pm i\tilde{\omega}_\mathrm{m}$. Since $|\lambda_0| \ll 1$ we expand the right hand side of eq.

(2.17) to linear order in λ and the resulting second order equation in λ gives

$$\lambda = -\frac{1}{2}\tilde{\gamma}_{\text{eff}} \pm i\tilde{\omega} \tag{2.18}$$

$$\tilde{\omega} = \sqrt{\tilde{\omega}_{\text{m}}^2 - \frac{\mathcal{K}}{1+\tilde{\Omega}^2}}, \quad \tilde{\gamma}_{\text{eff}} = \tilde{\gamma} + \mathcal{K}\frac{1-\tilde{\Omega}^2}{\left(1+\tilde{\Omega}^2\right)^2}. \tag{2.19}$$

Eq. (2.18) describes damped oscillations with frequency $\tilde{\omega}$ and effective damping $\tilde{\gamma}_{\text{eff}}$. The interesting feature here is that the effective damping might become negative when $\tilde{\Omega} > 1$. This happens if the coupling strength $\mathcal{K}$ is strong enough to overcome the intrinsic mechanical damping $\mathcal{K}(\tilde{\Omega}^2-1)/(1+\tilde{\Omega}^2)^2 > \tilde{\gamma}$. Thus, under these conditions the amplitude of mechanical oscillation is not damped but grows exponentially and the mechanical oscillation is unstable. Since the condition for the instability is independent of the mechanical frequency, the presented electromechanical coupling gives rise to a nonresonant mechanical instability.

2.6 Saturation mechanism

When a physical oscillator system becomes unstable, the amplitude will saturate due to nonlinear effects. At the saturation point of the amplitude, the rate at which energy is pumped into the system equals the rate of dissipation. When the saturation point is reached the system stabilises in a stationary state. There are two principal ways in which the saturation point can be reached. Either the efficiency of the pumping mechanism decreases with increasing amplitude or the damping processes increases with amplitude, fig. 2.2.

2.6.1 Nonlinear potential

Instabilities due to resonant pumping as in parametric resonance, the amplitude will saturate due to e.g. a Duffing nonlinearity described in eq. (2.8). The reason for the saturation is that the increased amplitude of oscillation results in an effective mechanical frequency $\omega \approx \omega_{\text{m}}^2 + \eta\langle(x/l)^2\rangle$, with time average $\langle\ldots\rangle$, which deviates further and further from ω_{m}. Hence, the resonance condition will be violated with increasing amplitude and the efficiency of the pumping mechanism will decrease, corresponding to the solid lines in fig. 2.2.

2.6.2 Nonlinear dissipation

In case of a nonresonant pumping mechanism the shift of the mechanical frequency does not affect the pumping efficiency. Therefore, the saturation mechanism has to be of another kind. One possible mechanism of saturation for nonresonant pumping is nonlinear dissipation. One simple way to model nonlinear dissipation is to replace

$$\gamma x \to \left(\gamma_L + \gamma_{NL}\left(\frac{x}{l}\right)^2\right)x \tag{2.20}$$

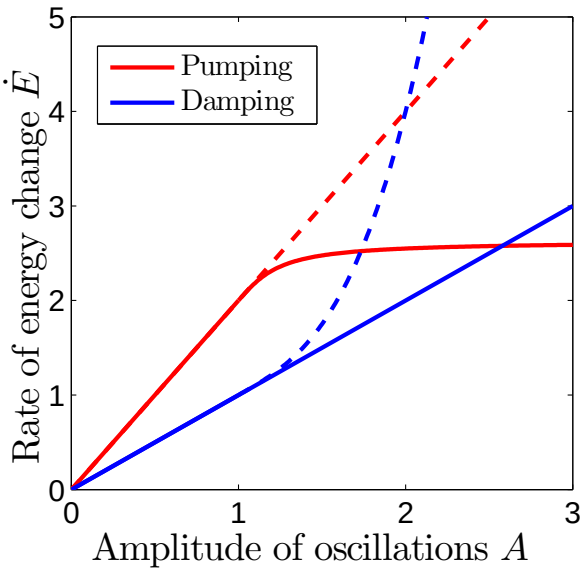

Figure 2.2: Schematic description of saturation mechanisms of systems in the unstable region. The amplitude of oscillations can either saturate due to a decreasing efficiency of the pumping mechanism (solid lines) or an enhanced damping mechanism (dashed lines).

in the equation of the mechanical dynamics. At small amplitudes $x \ll l$ the linear damping dominates but when the amplitude increases the nonlinear dissipation increases the efficiency of the damping mechanism. This situation is schematically pictured by the dashed lines in fig. 2.2. The stationary amplitude can be approximately calculated by perturbation theory [31].

Nonlinear dissipation as in eq. (2.20) has been used to theoretically model experimental results for graphene and CNT oscillators [32]. The physical origin of nonlinear dissipation is still unclear and might depend on the specific device. Some of the candidates for nonlinear dissipation include nonlinear clamping losses, sliding between the carbon oscillator and the substrate, nonlinear phonon-phonon interaction and interaction between in-plane and out-of-plane vibrations [33].

Chapter 3

Electromechanical interaction in isolated graphene oscillators

In the second article the model system was slightly adjusted, fig. 3.1. The system simply consists of a large doped graphene sheet suspended over a relatively narrow trench and there are no bulk electrodes. The gate electrodes still introduce the same kind of feedback mechanism to the mechanical vibration but are at a larger distance from the graphene membrane. The capacitive coupling between the membrane and the gates is therefore disregarded. The external electrical field is assumed to be polarized perpendicularly to the graphene sheet and to be spatially homogeneous. The dynamics is assumed to be homogeneous in the y-direction.

One important difference in comparison with the integrated resonators is that the electronic transport now is purely determined by internal properties of the graphene sheet and not by an external circuit. The transport properties of the graphene membrane may in some cases be affected by the substrate to which it is clamped. However, the graphene sheet is assumed to be isolated in the sense that the conductivity of the sheet is unaffected by the substrate of the suspension.

3.1 Electrodynamics - conductivity of graphene

The electrodynamics of the graphene sheet is described by a simple semiclassical hydrodynamic model. Firstly, the continuity equation

$$\frac{\partial}{\partial t}\rho(x,t) = -\frac{\partial}{\partial x}j(x,t) \tag{3.1}$$

assures conservation of charge density $\rho(x,t)$, and $j(x,t)$ is the current density. Further, an electrical field $E_{||}(x,t)$ along the membrane induces a charge flow which is assumed [34] to be related by

$$\frac{\partial}{\partial t}j(x,t) + \nu j(x,t) = \frac{1}{\mathcal{L}}E_{||}(x,t), \quad \frac{1}{\mathcal{L}} = \frac{e^2 v_{\mathrm{F}}\sqrt{n}}{\hbar^2\pi}, \tag{3.2}$$

where ν is the relaxation frequency, n is the surface density of electrons and v_{F} is the Fermi velocity of graphene.

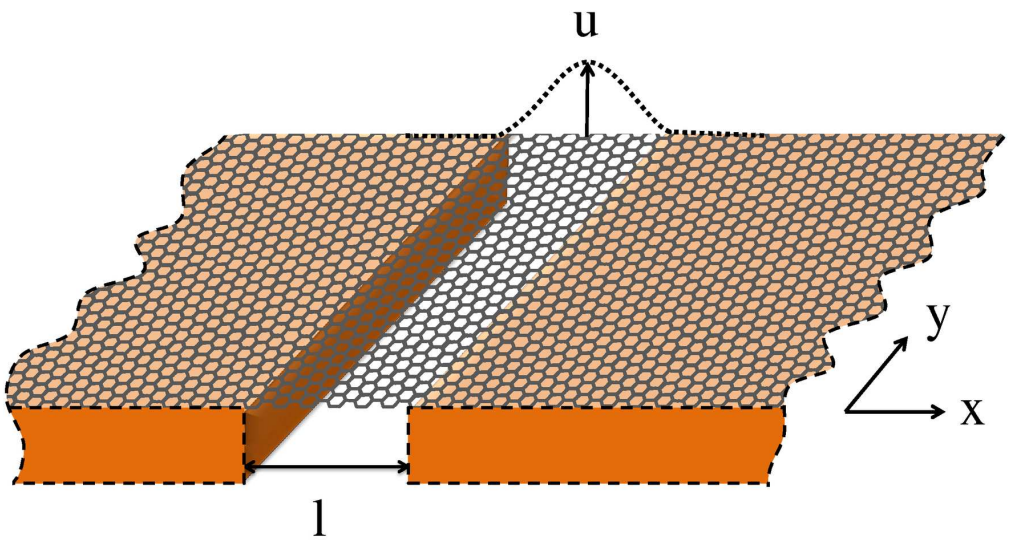

Figure 3.1: Cross-section of an infinite graphene sheet suspended over a trench with width l. The membrane can deflect vertically in the trench.

There is one external and one internal contribution to the electrical field along the sheet $E_{||}(x,t) = E_{\text{ext}}(t,x) + E_{\text{int}}(t,x)$. The external component is induced by the external gate field $E(t)$ when the membrane is deflected $E_{\text{ext}}(t,x) = E(t)\partial u(x,t)/\partial x$. The internal component is due to spatial variations in the charge density which generate a non-local interaction of the charge according to

$$E_{\text{int}}(t,x) = \frac{1}{2\pi\varepsilon_0}\mathcal{P}\int_{-\infty}^{\infty}\frac{\rho(x_1,t)}{x-x_1}\mathrm{d}x_1 \tag{3.3}$$

with vacuum permittivity ε_0 and $\mathcal{P}\int$ denotes the principal value of the integral. The internal field gives rise to a restoring force which can be viewed as a self-capacitance of the membrane.

Combining eqs. (3.1) and (3.2) gives an equation for how the charge density responds to an external field

$$\frac{\partial^2}{\partial t^2}\rho(x,t) + \nu\frac{\partial}{\partial t}\rho(x,t) + \frac{1}{2\pi\varepsilon_0\mathcal{L}}\frac{\partial}{\partial x}\mathcal{P}\int_{-\infty}^{\infty}\frac{\rho(x_1,t)}{x-x_1}\mathrm{d}x_1 = -\frac{E(t)}{\mathcal{L}}\frac{\partial^2}{\partial x^2}u(x,t). \tag{3.4}$$

The charge waves generated by the homogeneous external electrical field is described by eq. (3.4). The charge waves can be thought of as to be generated by two point sources at the trench edges since the second derivative of the vibrational profile has sharp maxima at the clamping points, see right hand side of eq. (3.4). The induced charge waves interfere constructively in the suspended region, at certain frequencies of the external field, establishing geometrical resonance with the vibrational modes above the trench.

3.2 Electromechanical feedback on mechanical oscillation

The mechanical motion of the membrane is again described by eq. (2.5) with pressure $F = E(t)\rho(x,t)$. For the isolated oscillator, several vibrational modes will be considered. This is because the induced space variations of the charge distribution are on the length scale l. The equations for the different mechanical modes are obtained by projecting eq. (2.5) on the different modes $\Phi_n(x)$, here indicated by $\langle ... \rangle$,

$$\ddot{\zeta}_n(t) + \gamma\zeta_n(t) + \omega_n^2\zeta(t) = \frac{E(t)}{\rho_g}\langle \Phi_n(\xi), \rho(\xi,t)\rangle. \tag{3.5}$$

The frequencies can conviniently be expressed by $\omega_n = \omega_M^2 K_n^2$. The frequency is given by $\omega_M = \pi\sqrt{T_0/\rho_m}/l$ and the wave numbers K_n are obtained from

$$\left(-\frac{1}{\pi^2}\frac{\partial^2}{\partial\xi^2} + b\frac{\partial^4}{\partial\xi^4}\right)\Phi_n(\xi) = K_n^2\Phi_n(\xi). \tag{3.6}$$

The feedback in eqs. (3.5) and (3.4) are analysed in a similar manner as the feedback in chapter 2 by writing an integral expression for the charge density and substitute it into eq. (3.5). For details of the procedure the reader is referred to paper III. The analysis leads to the perturbed complex frequencies

$$\begin{aligned}
\omega_n &= \omega_M\left[K_n + \frac{\varepsilon^2}{K_n}\Lambda_n(\tilde{\Omega}) + \frac{i}{2}\left(\frac{\gamma}{\omega_M} + \frac{\varepsilon^2\tilde{\omega}_M}{K_n}\eta_n(\tilde{\Omega})\right)\right] \\
\Lambda_n\left(\tilde{\Omega}\right) &= \int_{-\infty}^{\infty}\Lambda(\tilde{\Omega},q)w_n(q)dq, \\
\eta_n\left(\tilde{\Omega}\right) &= \int_{-\infty}^{\infty}\eta(\tilde{\Omega},q)w_n(q)dq.
\end{aligned} \tag{3.7}$$

where $\tilde{\nu} = \nu/\omega_p$, $\tilde{\omega}_M = \omega_M/\omega_p$ and $\tilde{\Omega} = \Omega/\omega_p$ are dimensionless frequencies and coupling constant $\varepsilon = E_0\sqrt{\varepsilon_0/2\pi l\rho_g}/\omega_M$. The functions $\Lambda(\tilde{\Omega},q)$ and $\eta(\tilde{\Omega},q)$ are given by

$$\Lambda(\tilde{\Omega},q) = \tfrac{1}{2}\frac{\tilde{\Omega}^2 - |q|}{\left(|q|-\tilde{\Omega}^2\right)^2 + \tilde{\nu}^2\tilde{\Omega}^2} \tag{3.8}$$

$$\eta(\tilde{\Omega},q) = -\tilde{\nu}\frac{(|q|+\tilde{\Omega}^2)^2 - \tilde{\nu}\tilde{\Omega}^2(4\tilde{\Omega}^2+\tilde{\nu}^2)}{\left(\left(|q|-\tilde{\Omega}^2\right)^2 + \tilde{\nu}^2\tilde{\Omega}^2\right)^2} \tag{3.9}$$

and $w_n(q) = (\pi q)^2|\langle e^{i\pi qx/l}, \Phi_n(x)\rangle|^2$. An interpretation of the influence of the electromechanical coupling on the frequencies will be discussed in chapter 5.

Chapter 4

Electromechanical interaction in movable quantum dot systems

Two classical models describing the nonresonant instability mechanism in graphene based electromechanical oscillators were introduced in chapters 2 and 3. This chapter introduces a quantum mechanical model of a movable single-electron quantum dot. In such systems the quantum nature of electrons are well pronounced and the charge on the oscillator can no longer be described as a classical quantity.

4.1 Quantum dynamics

One of the most famous equations in physics is the Schrödinger equation which describes how the state of a quantum system evolves over time. The time evolution is determined by the Hamiltonian $\hat{H}$ of the system which is a hermitian quantum operator corresponding to the total energy of the system. If the initial quantum state is known the succeeding state at a later time can be predicted. However, when a physical quantity is measured, the result can in general not be predicted with certainty. This can only be done if the measured quantum state happens to be in an eigenstate of the observable which corresponds to the physical quantity. In the other more common situation only the expectation value of the outcome can be predicted. If the system is initialised in exactly the same way and the experiment is carried out several times the mean value of the measured results will approach the predicted expectation value. However, every individual measurement can only yield an eigenvalue of the observable.

In many cases the initial quantum state is not known because of the complexity of the system. A more general and useful formalism in this situation is to use the density operator $\hat{\rho}$. The density operator is a quantum mechanical operator which describes the state of the system. The advantage is that the density operator can not only describe the evolution of a pure state, as in the Schrödinger formalism, it can also describe mixed states. The time evolution of the density operator is given by

the quantum Liouville equation

$$i\hbar\frac{\partial}{\partial t}\hat{\rho} = \left[\hat{H},\hat{\rho}\right] \tag{4.1}$$

which can be derived from the Schrödinger equation. The expectation value of a physical quantity corresponding to the operator $\hat{A}$ is evaluated by taking the trace over the observable weighted by the density operator

$$\langle\hat{A}\rangle = \mathrm{Tr}(\hat{A}\hat{\rho}). \tag{4.2}$$

Another advantage with the density operator formalism is that we, in a neat way, can take into account special types of interactions with the environment which contains a huge amount of degrees of freedom. The idea is to reduce the dynamics of the total density operator to the relevant degrees of freedom. The interaction with the environment can then be taken into account via superoperators. One example is the Lindblad superoperator which describes linear dissipative coupling to an environmental bath.

In many situations it is useful to view the total quantum system as consisting of several subsystems, in our case the mechanical and electrical subsystems. The environment which is a third subsystem is taken into account by the superoperator approach. If the subsystems are separated with no interaction the density operator can be written as a product state of the subsystems $\hat{\rho}_{\mathrm{tot}} = \hat{\rho}_1 \otimes \hat{\rho}_2$. However, if there is an interaction between the subsystems the density operator is in general not in a product state but in an entangled state of the two subsystems. Entanglement is a pure quantum mechanical phenomenon with no classical analogue. However, entangled states dephases and decays due to the coupling between the quantum system and the environment. This is the main reason for why many quantum phenomena are 'washed out' at the macroscopic scale.

4.2 Hamiltonian of the system

The system under consideration is a movable single-electron quantum dot (QD), fig. 4.1. It is assumed to be in tunnel contact with grounded bulk electrodes with continuous density of electronic states. The dot is suspended and may perform oscillations in the vertical direction between the gate electrodes. An ac-electrical field is applied between the gate electrodes which adjusts the electrical potential on the QD if the QD is deflected from the flat position. The potential difference between the QD and the bulk electrodes will alter the charge occupation on the QD. At the same time the electrical field will exert a vertical force on the charged QD influencing the mechanical motion. Hence, there is an electromechanical feedback in the system, very similar to the feedback studied in chapters 2 and 3.

4.2.1 Mechanical Hamiltonian

For the mechanical dynamics the same procedure as in chapter 2 could formally be performed for a quantum mechanical system to find the eigenmodes of vibrations.

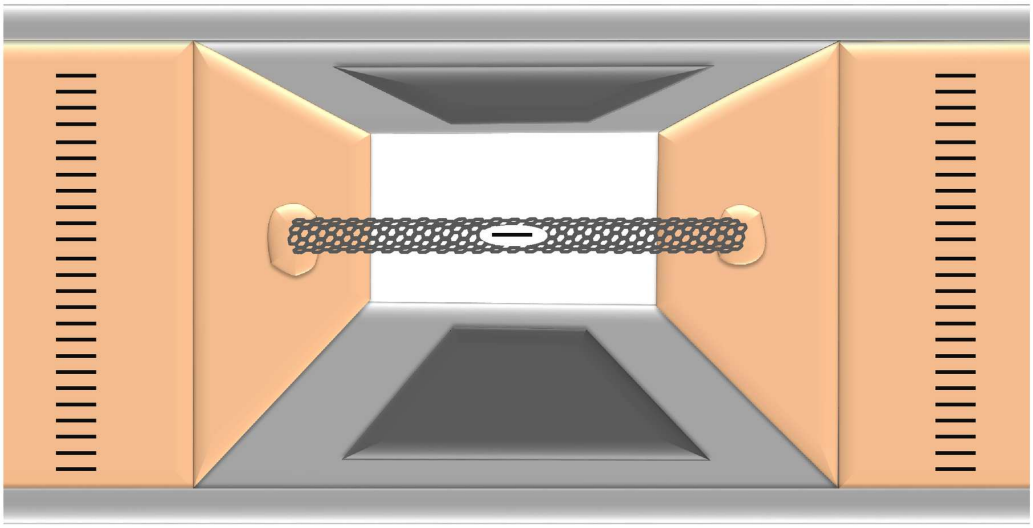

Figure 4.1: The QD on a suspended CNT is free to move vertically. An ac-voltage applied to the dark grey gate electrodes introduces an electromechanical coupling between the mechanical vibration and the electronic subsystem. The black bars indicate electronic states.

However, for simplicity the mechanical dynamics will be described as a quantum mechanical harmonic oscillator.

The dynamics of the harmonic oscillator is characterised by the Hamiltonian

$$\hat{H}_{\mathrm{m}} = \hbar\omega_{\mathrm{m}}\hat{c}^{\dagger}\hat{c}, \tag{4.3}$$

with bosonic raising and lowering operators $\hat{c}^{\dagger}$ and $\hat{c}$, respectively. These operators increase and decrease the number of vibrational quanta with energy $\hbar\omega_{\mathrm{m}}$. The raising and lowering operators relate to the position and momentum operators as

$$\hat{x} = a_0\left(\hat{c}^{\dagger} + \hat{c}\right), \quad \hat{p} = ima_0\omega_{\mathrm{m}}\left(\hat{c}^{\dagger} - \hat{c}\right) \tag{4.4}$$

where $a_0 = \sqrt{\hbar/(2m\omega_{\mathrm{m}})}$ and m is the effective mass of the oscillator. The quantity $a_0 = \sqrt{\langle\hat{x}^2\rangle}$ is the amplitude of zero-point fluctuations in the ground state of the oscillator.

4.2.2 Electronic tunnelling Hamiltonian

The electronic subsystem consists of the single-level quantum dot, the bulk electrodes and the tunnel coupling between them. The ac-electrical field is assumed to consist of a large amount of photon quanta and to be unaffected by absorption and emission from the system. Therefore, the ac-field will only show up as a classical coupling field in the electromechanical interaction.

A quantum dot is a physical object which exhibits quantum mechanical properties. It is usually made of a semiconducting material at the length scale of typically 10 nm. Due to the spatial confinement the energy levels of the system are separated,

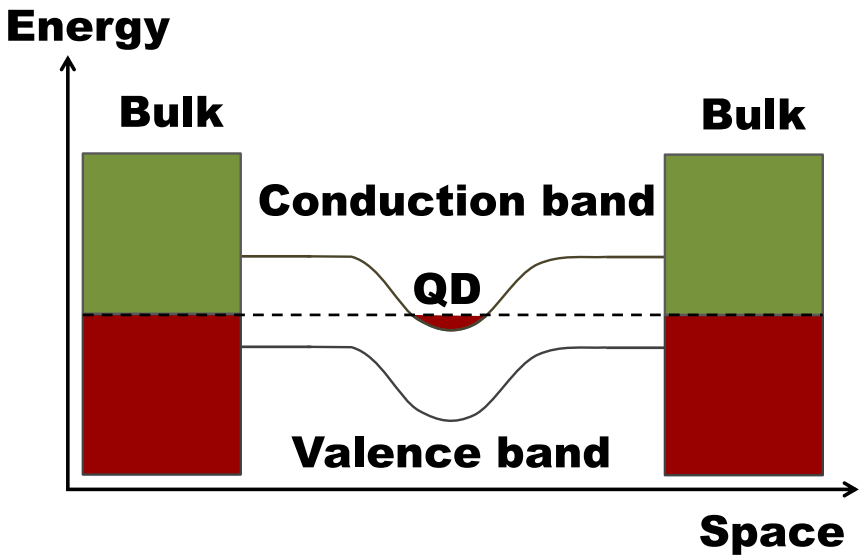

Figure 4.2: The semiconducting CNT can be tuned into a QD by locally applying a dc-voltage on the gate electrodes. The conduction band can by this means be lowered below the Fermi level of the bulk electrodes which creates a single electron confinement.

manifesting the quantum nature of the object. It is very improbable that the QD is populated by two electrons simultaneously, because of the huge Coulomb energy the confinement would lead to. There are many different realisations of single-level quantum dots. The picture to have in mind here is a suspended carbon nanotube (CNT) clamped to a conducting substrate [5], fig. 4.2. Due to the effects discussed above the CNT is assumed to only be occupied by a maximum of one electron at a time. The energy of the state is denoted ε_0 and the state corresponds to the creation and annihilation operators $\hat{d}^\dagger$ and $\hat{d}$, respectively.

The conducting substrate serves as a reservoir for electrons which can tunnel to and from the QD. Surface effects will be neglected and the reservoir will be treated as a bulk electrode with density of states ν. The dynamical processes which take place in the system is assumed to occur only in the close vicinity of the Fermi energy $E_F \sim \varepsilon_0$ of the bulk electrodes, due to well separated energy scales. The density of states $\nu = \nu(E_F)$ is therefore approximated to be constant. The creation and annihilation operators which correspond to the bulk state $|\varepsilon\rangle$ with energy ε are denoted $\hat{l}_\varepsilon^\dagger$ and $\hat{l}_\varepsilon$, respectively.

The bulk states are coupled to the dot state via quantum-tunnelling transitions. Tunnelling processes can be described by terms such as $\mathcal{T}\hat{d}^\dagger\hat{l}_\varepsilon$ and its hermitian conjugate, where $\mathcal{T}$ is a measure of the coupling strength. It represents the energy 'gained' when the electron delocalises between the coupled states. The tunnelling strength $\mathcal{T}$ is a characteristic of the spatial overlap between the involved wave functions in the uncoupled systems. However, for simplicity also $\mathcal{T}$ is assumed to be constant. The operator $\hat{d}^\dagger\hat{l}_\varepsilon$ will annihilate an electron in the state $|l_\varepsilon\rangle$ and create an

electron in the state $|d\rangle$. In total the number of electrons is conserved. If the state $|\varepsilon\rangle$ is empty or if $|d\rangle$ is already populated the term is annihilated as a definition of the fermionic operators.

The Hamiltonian of the electronic subsystem which describes the bulk electrodes, the single quantum dot and the tunnel coupling takes the form

$$\hat{H}_{\mathrm{el}} = \int \mathrm{d}\tilde{\varepsilon}\nu\tilde{\varepsilon}\hat{l}^{\dagger}_{\tilde{\varepsilon}}\hat{l}_{\tilde{\varepsilon}} + \varepsilon_0\hat{d}^{\dagger}\hat{d} + \nu\mathcal{T}\int \mathrm{d}\tilde{\varepsilon}\left(\hat{l}^{\dagger}_{\tilde{\varepsilon}}\hat{d} + \hat{l}_{\tilde{\varepsilon}}\hat{d}^{\dagger}\right). \tag{4.5}$$

The combination $\hat{d}^{\dagger}\hat{d}$ can be viewed as probing if the fermionic state $|d\rangle$ is populated, by annihilating it and creating it again adding the energy ε_0 to the total energy. If the state $|d\rangle$ is empty the term annihilates and gives zero contribution to the total energy.

Due to the tunnelling term the states $|\varepsilon\rangle$ and $|d\rangle$ will no longer be eigenstates of the electronic subsystem but will hybridise into a new set of eigenstates of the coupled system. The diagonalised form of the Hamiltonian (4.5) is

$$\hat{H}_{\mathrm{el}} = \int \mathrm{d}\varepsilon\nu\varepsilon\hat{\psi}^{\dagger}_{\varepsilon}\hat{\psi}_{\varepsilon}, \tag{4.6}$$

with creation (annihilation) operators of the hybridised Fermi sea $\psi^{\dagger}_{\varepsilon}$ (ψ_{ε}) corresponding to the level with energy ε. The density of states in the hybridised system is taken to equal ν since the single-level state only gives a minor correction. The rate $\Gamma = \pi\mathcal{T}^2\nu/\hbar$ is the tunnelling frequency between the dot and electrodes. It describes the characteristic time an electron survives on the QD before it relaxes to the bulk electrodes.

4.2.3 Electromechanical interaction Hamiltonian

In most situations, as in our model, the interesting physics is governed by the interaction between the subsystems. With zero external electrical field the mechanical and electrical Hamiltonians fulfil $[\hat{H}_{\mathrm{m}}, \hat{H}_{\mathrm{el}}] = 0$ meaning that the subsystems are non-interacting and can be analysed separately. But when the electrical field is turned on, the spatial position of the QD will determine the energy of the dot state relative to the bulk electrodes. If the dot state is deflected from the flat position it will correspond to a shift in the energy of the state according to

$$\varepsilon_0\hat{d}^{\dagger}\hat{d} \rightarrow (\varepsilon_0 + eE(t)\hat{x})\hat{d}^{\dagger}\hat{d} \tag{4.7}$$

where $E(t) = E\cos(\Omega t)$ is the electrical field between the gate electrodes. The unperturbed term $\varepsilon_0\hat{d}\,\dagger\,\hat{d}$ is taken into account by eq. (4.6). The perturbation introduces an electromechanical coupling in the Hamiltonian

$$\hat{H}_{\mathrm{int}} = eE_0a_0\cos(\Omega t)(\hat{c}^{\dagger} + \hat{c})\hat{d}^{\dagger}\hat{d}. \tag{4.8}$$

The dot operators can be expressed in the diagonalised basis according to

$$\hat{d}^{\dagger} = \int \mathrm{d}\varepsilon b(\varepsilon)\hat{\psi}^{\dagger}_{\varepsilon}, \quad b(\varepsilon) = \nu\frac{\mathcal{T}}{\varepsilon - \varepsilon_0 + i\hbar\Gamma}. \tag{4.9}$$

The dynamics of the electromechanical system is governed by its total Hamiltonian $\hat{H} = \hat{H}_{\mathrm{m}} + \hat{H}_{\mathrm{el}} + \hat{H}_{\mathrm{int}}$ together with the dissipative coupling to the environment.

4.2.4 Dissipation mechanisms

As mentioned in the beginning of this section, it is in many cases possible to describe the interaction with the environment by superoperators. Dissipative couplings to the environment will be considered both for the bosonic mechanical subsystem as well as for the fermionic electronic subsystem.

Dissipation in mechanical subsystem

One of the most common dissipation operators in bosonic systems is the Lindblad superoperator

$$\mathcal{L}_{\mathrm{L}}(\hat{\rho}) = \gamma_{\mathrm{L}} \left((\bar{n}+1) \left(\hat{c}\hat{\rho}\hat{c}^{\dagger} - \frac{1}{2}\{\hat{c}^{\dagger}\hat{c}, \hat{\rho}\} \right) + \bar{n} \left(\hat{c}^{\dagger}\hat{\rho}\hat{c} - \frac{1}{2}\{\hat{c}\hat{c}^{\dagger}, \hat{\rho}\} \right) \right) \tag{4.10}$$

with coupling strength γ_{L}, average number of bosons in the thermal bath $\bar{n}$ given by the Bose-Einstein distribution and anti-commutator $\{\hat{A}, \hat{B}\} = \hat{A}\hat{B} + \hat{B}\hat{A}$. The Lindblad superoperator can be derived from Liouvillian dynamics of the total system fulfilling the Liouville eq. (4.1) [35]. The Lindblad superoperator describes dissipative single-quanta processes where one vibron is added or annihilated. If no external forces bring the subsystem out of equilibrium it will thermalise due to these processes and adjust to the temperature of the environmental bath. Such single-vibron interaction gives rise to linear dissipation of the mechanical motion with respect to the amplitude of actuation.

Multi-vibron processes can be described by the superoperator [36]

$$\mathcal{L}_{\mathrm{NL}}(\hat{\rho}) = \gamma_{\mathrm{NL}} \left((\bar{n}+1) \left(\hat{c}\hat{c}\hat{\rho}\hat{c}^{\dagger}\hat{c}^{\dagger} - \frac{1}{2}\{\hat{c}^{\dagger}\hat{c}^{\dagger}\hat{c}\hat{c}, \hat{\rho}\} \right) + \bar{n} \left(\hat{c}^{\dagger}\hat{c}^{\dagger}\hat{\rho}\hat{c}\hat{c} - \frac{1}{2}\{\hat{c}\hat{c}\hat{c}^{\dagger}\hat{c}^{\dagger}, \hat{\rho}\} \right) \right) \tag{4.11}$$

with coupling strength γ_{NL}. It describes processes where two vibrons are either created or annihilated at the same time. Multi-vibron processes give rise to nonlinear dissipation of the mechanical motion with respect to the amplitude of actuation. Further, off-diagonal elements in the density operator are assumed to dephase on a very short time scale.

Dissipation in electronic subsystem

For the electronic subsystem no explicit form of the dissipation will be considered. Instead, the electronic subsystem is assumed to only be slightly perturbed from its equilibrium. Internal processes is assumed to quickly force the electronic subsystem back to equilibrium at some temperature T whenever its distribution is perturbed. This approximation allows for the separation of the density operator into a product state $\hat{\rho}(t) = \hat{\rho}_{\mathrm{m}}(t) \otimes \hat{\rho}_{\mathrm{eq}}$ of the mechanical density operator $\hat{\rho}_{\mathrm{m}}$ and the equilibrium electronic density operator $\hat{\rho}_{\mathrm{eq}}$, $[\hat{H}_{\mathrm{el}}, \hat{\rho}_{\mathrm{eq}}]$. This is known as the Born approximation.

4.3 Dynamics of the pumping mechanism

The electromechanical interaction in the system may lead to a pumping mechanism of mechanical vibrations. To see this, let us investigate the quantum dynamics of the coupled system governed by the dissipative Liouville equation

$$i\hbar\frac{\partial}{\partial t}\hat{\rho} = \left[\hat{H}_{\rm m}+\hat{H}_{\rm el}+\hat{H}_{\rm int},\hat{\rho}\right]+i\hbar(\mathcal{L}_{\rm L}(\hat{\rho})+\mathcal{L}_{\rm NL}(\hat{\rho})). \tag{4.12}$$

The analysis of this equation will be limited to high-frequency driving of the electrical field $\Omega\sim\Gamma\gg\omega_{\rm m}$. The dissipative terms drives the mechanical density operator towards its equilibrium distribution at the temperature of the mechanical environmental bath $T_{\rm m}$. On the other hand, the external driving which couples the mechanical and electrical dynamics induces processes which drives the system away from the equilibrium. The possible transition processes from the interaction term

$$\hat{H}_{\rm int}=\frac{eEa_0}{2}\left(e^{i\Omega t}+e^{-i\Omega t}\right)(\hat{c}^\dagger+\hat{c})\int{\rm d}\varepsilon\int{\rm d}\varepsilon'\nu^2\frac{\mathcal{T}^2}{(\varepsilon-\varepsilon_0+i\hbar\Gamma)(\varepsilon'-\varepsilon_0-i\hbar\Gamma)}\hat{\psi}^\dagger_\varepsilon\hat{\psi}_{\varepsilon'}. \tag{4.13}$$

are schematically pictured in fig. 4.3.

To analyse the transitions that are induced by the electromechanical coupling, let us at first assume the hybridised Fermi sea to be at zero temperature $T=0$. If so, all electronic states below the hybridised Fermi surface $E_{\rm F}$ is populated and all states above the surface are empty. In this case only processes with stimulated absorption from the driving field are possible since each transition has to conserve energy and $\Gamma\gg\omega_{\rm m}$. During the stimulated absorption process one electron in the hybridised Fermi sea is annihilated by $\hat{\psi}_{\varepsilon'}$ and recreated above the Fermi sea surface in an empty state by $\hat{\psi}_\varepsilon$. Simultaneously, one vibrational quantum is either annihilated by $\hat{c}$ or created by $\hat{c}^\dagger$. If the temperature of the hybridised Fermi sea is increased $T>0$, the occupation probability near the Fermi sea level is smeared. This opens transition channels for stimulated emission of electromagnetic quanta back to the driving field. These processes are reversed with respect to the electronic subsystem but still involve both creation or annihilation of vibrational quanta.

Since the interaction changes the number of vibrational quanta $\mathcal{N}$, it might give rise to an instability of the mechanical subsystem depending on the rates of the different processes. In Appendix C these rates are derived

$$\Gamma^{\pm\omega_{\rm m}}_{\pm\Omega}=\frac{(eEa_0)^2}{2\pi\hbar^2\Gamma}\int{\rm d}\varepsilon{\rm d}\varepsilon'\nu^2 n_{\rm f}(\varepsilon)\Big(1-n_{\rm f}(\varepsilon')\Big)\frac{(\hbar\Gamma)^3\delta(\varepsilon'-\varepsilon\pm\hbar\Omega\pm\hbar\omega_{\rm m})}{\left|\varepsilon_\alpha-\varepsilon_0+i\hbar\Gamma\right|^2\left|\varepsilon'-\varepsilon_0+i\hbar\Gamma\right|^2}, \tag{4.14}$$

where $n_{\rm f}$ is the fermi dirac distribution. The pluses refer to creation of vibrational quantum, in the driving field and mechanical vibration, respectively. Analogously, a minus sign refers to the decrease of one quantum of the relevant oscillation.

The rate equation for the stationary part of the density operator also derived in Appendix C, takes the form

$$\Gamma^-\left(\hat{c}\hat{\rho}_{\rm st}\hat{c}^\dagger-\hat{c}^\dagger\hat{c}\hat{\rho}_{\rm st}\right)+\Gamma^+\left(\hat{c}^\dagger\hat{\rho}_{\rm st}\hat{c}-\hat{c}\hat{c}^\dagger\hat{\rho}_{\rm st}\right)+\hat{\mathcal{L}}_{\rm L}(\hat{\rho}_{\rm st})+\hat{\mathcal{L}}_{\rm NL}(\hat{\rho}_{\rm st})=0, \tag{4.15}$$

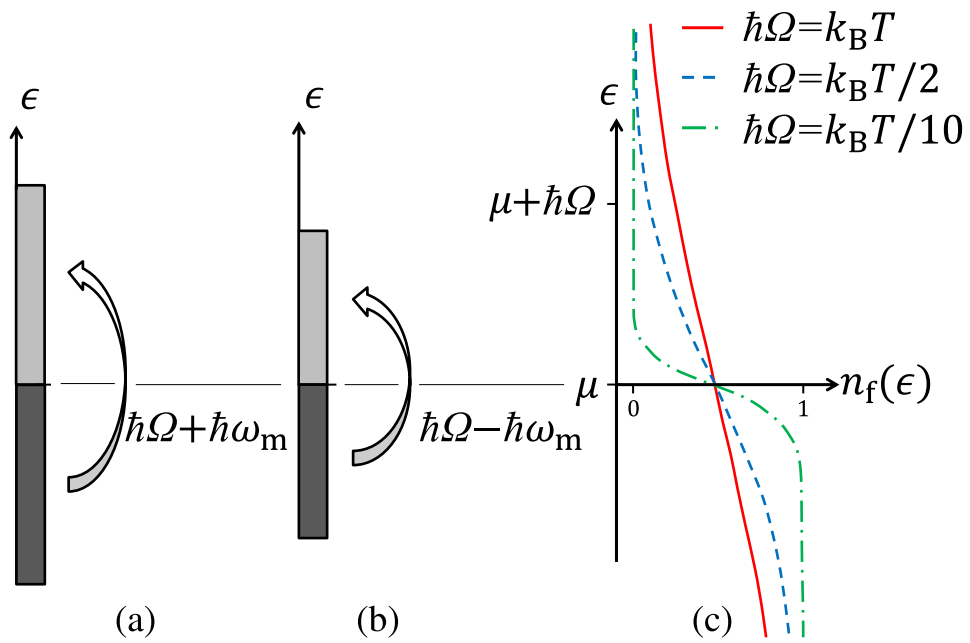

Figure 4.3: Dark (light) grey areas represents initial (final) states of the electrons which are affected by the interaction processes at zero temperature. During the stimulated absorption of the electromagnetic field the vibration of the QD is either (a) decreased with one vibrational quantum or (b) increased with one vibrational quantum. The Fermi-Dirac occupation probability $n_{\mathrm{f}}(\varepsilon)$ is smeared with increasing temperature (c). The smearing opens up channels for stimulated emission back to the electromagnetic field.

with rates $\Gamma^{-} = \Gamma^{-\omega_m}_{+\Omega} + \Gamma^{-\omega_m}_{-\Omega}$ and $\Gamma^{+} = \Gamma^{+\omega_m}_{+\Omega} + \Gamma^{+\omega_m}_{-\Omega}$. To analyse the rate equation and seek for an instability, let us assume that the multi-vibron dissipation mechanism can be neglected close to the ground state of the mechanical oscillator. The average number of mechanical quanta $\mathcal{N}$ diverges if the pumping processes overcome the damping processes $\Gamma^{+} > \gamma_L + \Gamma^{-}$. According to the results presented in the following chapter, such a mechanical instability is present.

Chapter 5

Summary of results and discussion

In this chapter I summarise the main results from the papers and compare some of the features. The nature of the nonresonant excitation mechanism is the same in all three papers and the main difference is the models of the electronic subsystem used in the separate cases. Due to the robustness of the mechanism it is expected to be present in a large range of nanoelectromechanical devices and not only in the specific cases mentioned as model systems in the papers.

5.1 Nonresonant pumping region

The studied electromechanical instability is nonresonant in the sense that the criteria for the driving frequency is independent of the mechanical frequency. Below follows a discussion of how the pumping region depends on the driving frequency.

5.1.1 Pumping of the integrated graphene oscillator

The nonresonant instability of the integrated graphene oscillator is due to the feedback coupling of the electromechanical motion. The time delay of the charge response to the driving field generates a feedback which renormalises the frequency of the mechanical vibration. The focus of this thesis is the fact that the interaction also affects the effective mechanical damping

$$\gamma = \omega_{\mathrm{m}} \left(\frac{1}{Q} + \varepsilon\zeta \right) \tag{5.1}$$

$$\varepsilon = \frac{C_{\mathrm{G}}(0) V_{\mathrm{G}}^2}{2md^2 \nu_{RC(0)} \omega_{\mathrm{m}}}, \quad \zeta = \eta \frac{1 + (1-\eta)^2 \tilde{\Omega}^2}{1 + \tilde{\Omega}^2} \frac{1 - \tilde{\Omega}^2}{\left(1 + \tilde{\Omega}^2\right)^2}. \tag{5.2}$$

The damping shift $\varepsilon\zeta$ is the product of the coupling strength ε and the normalised damping shift ζ which depends on geometry and driving frequency. The factor ζ decreases with the capacitance ratio $\eta = C_{\mathrm{G}}(0)/C(0)$ manifesting the fact that a substantial part of the charge on the membrane has to be situated above the gate electrode to have a pronounced interaction. The frequency dependence of the normalised damping shift ζ is shown in fig. 5.1. The sign of ζ changes when the driving

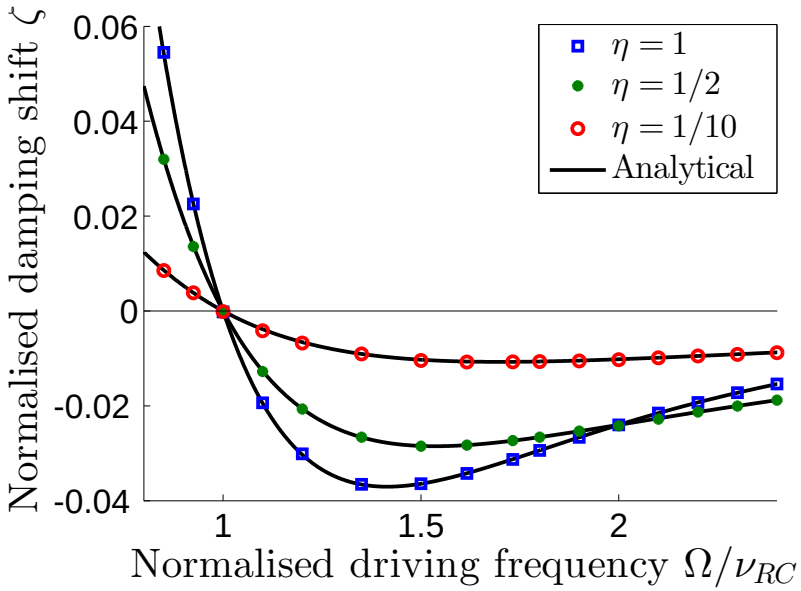

Figure 5.1: The damping shift becomes negative when the driving frequency exceeds the inverse retardation time $\nu_{RC(0)} = 1/RC(0)$. The markers indicate damping shift obtained from direct simulations of eq. (2.4) and eq. (2.11) with $x/d \sim \omega_m/\nu_{RC(0)} = 10^{-2}$.

frequency exceeds the RC-frequency of the integrated circuit $\Omega > \nu_{RC(0)}$. In this region the effect of the driving field is pumping of the mechanical motion. The most efficient pumping is achieved at driving frequency $\Omega \approx 3\nu_{RC(0)}/2$.

5.1.2 Pumping of the movable quantum dot

The electromechanical instability of the movable quantum dot is an interplay between the induced rates of increment $\Gamma^{+} = \Gamma_{-\Omega}^{+\omega_m} + \Gamma_{+\Omega}^{+\omega_m}$ and decrement $\Gamma^{+} = \Gamma_{-\Omega}^{-\omega_m} + \Gamma_{+\Omega}^{-\omega_m}$ of vibrational quanta. They can be calculated analytically in the case of temperature $T = 0$ of the hybridised Fermi sea,

$$\Gamma_{-\Omega}^{\pm\omega_m} = \frac{(eEa_0)^2}{\pi\hbar^2\Gamma}\chi\left(\frac{\Omega \mp \omega_m}{\Gamma}\right) \tag{5.3}$$

$$\chi(x) = \frac{x\arctan(x) + \ln\left(1+x^2\right)}{x\left(4+x^2\right)}. \tag{5.4}$$

At finite temperature, the rates can be calculated numerically, fig. 5.2. Very similar to the classical case there is a hump representing the pumping region slightly above $\Omega = \Gamma$. In the pumping region, the net effect of the induced processes is pumping of mechanical quanta, $\Gamma^{+} - \Gamma^{-} > 0$.

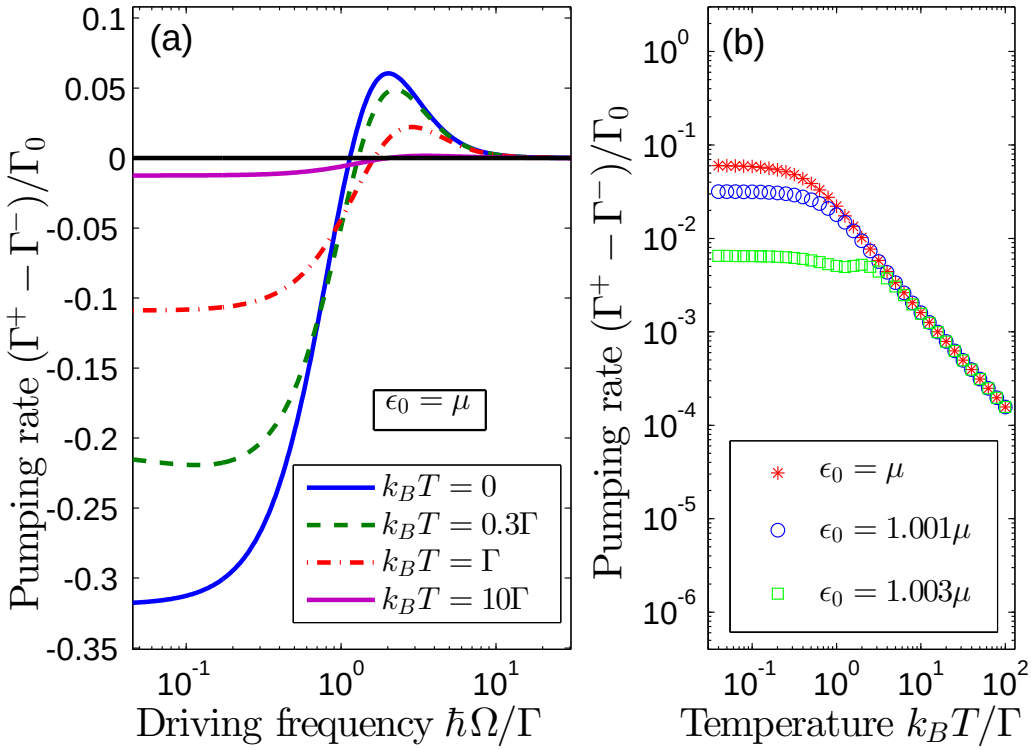

Figure 5.2: Pumping rate of mechanical quanta induced by the external field with $\Gamma_0 = (eEa_0)^2/(\hbar^2\Gamma)$. (a) At driving frequencies Ω slightly larger than the tunnelling frequency Γ, mechanical quanta are pumped into the vibration. (b) At temperatures $k_BT > \hbar\Gamma$, the smearing of the Fermi surface decreases the efficiency of the pumping mechanism. The pumping efficiency is symmetric with respect to $\Delta = \mu - \varepsilon_0$ and decreases when the single-level-state energy deviates from the chemical potential μ of the bulk electrodes. The plots are valid for $\hbar\Gamma/\mu = 10^{-3}$ and $\omega_m/\Gamma = 10^{-2}$.

5.2 Instability of the mechanical motion

In most instability mechanisms, the driving field has to exceed a critical value V_c above which the induced pumping overcomes the intrinsic damping in the system. This is also true for the nonresonant instability mechanism in the classical and quantum mechanical systems studied here. However, there is one important difference between the classical models and the quantum mechanical model. The induced quantum transitions simultaneously increase and decrease the vibration in a diffusive-like manner, whereas in the classical models the vibrational mode is either pumped or damped with no diffusive-like processes.

5.2.1 Instability of the integrated graphene oscillator

In the classical model in chapter 2, the influence from the driving field results in pure additional damping or pure pumping of the mechanical oscillator without any stochastic or diffusive force. At voltages $V_G < V_c$, the amplitude of oscillations is zero since the effective damping is positive. Above the critical voltage, the effective damping is negative and the amplitude increases abruptly until it is saturated by the nonlinear damping. In a less naive model one could include a stochastic force related to the intrinsic mechanical damping via the fluctuation dissipation theorem. The amplitude of oscillations would then not be zero but fluctuate around zero due to the stochastic force. If the mechanical damping is reduced by the electromechanical coupling, the relative importance of the fluctuation force would increase. This would lead to a larger mean square displacement of the oscillator even before the instability is reached. Further, the induced current will not be deterministic as assumed in paper I, but will exhibit shot noise which occurs due to the discrete nature of electrons. Such noise might be another source for diffusive dynamics of the oscillator. However, no diffusive dynamics were considered in the classical descriptions in neither paper I nor II.

An estimation of the critical gate voltage at which the instability is reached can be calculated by assuming $\eta = 0.5$ which gives $\zeta = -0.03$, gate capacitance $C_G(0) \approx \varepsilon_0 A/d$, mass of the oscillator $m = \rho_g A$, where A is the area of the oscillator and ρ_g the 2D-mass density of graphene. Further, let us consider the values $d = 100$ nm, $\omega_m = 10^8$ Hz, $Q = 10^4$, $\nu_{RC(0)} = 10^9$ Hz. These assumptions estimate the critical voltage to be $V_c = \sqrt{2\omega_m \nu_{RC(0)} \rho_g d^3 (|\zeta| Q \varepsilon_0)^{-1}} \approx 10$ mV.

5.2.2 Instability of the movable quantum dot

A mechanical instability of the quantum dot would manifest itself as a rapid increase of the average number of vibrational quanta $\mathcal{N}$ in the oscillation. In Appendix D, an expression for $\mathcal{N}$ is derived. In the quantum mechanical description both pumping and damping processes are induced simultaneously. The processes compete in the same diffusive way as the Lindblad dissipation. The behaviour of $\mathcal{N}$ is qualitatively different in the damping region $\Gamma^+ < \Gamma^- + \gamma_L$ and pumping region $\Gamma^+ > \Gamma^- + \gamma_L$.

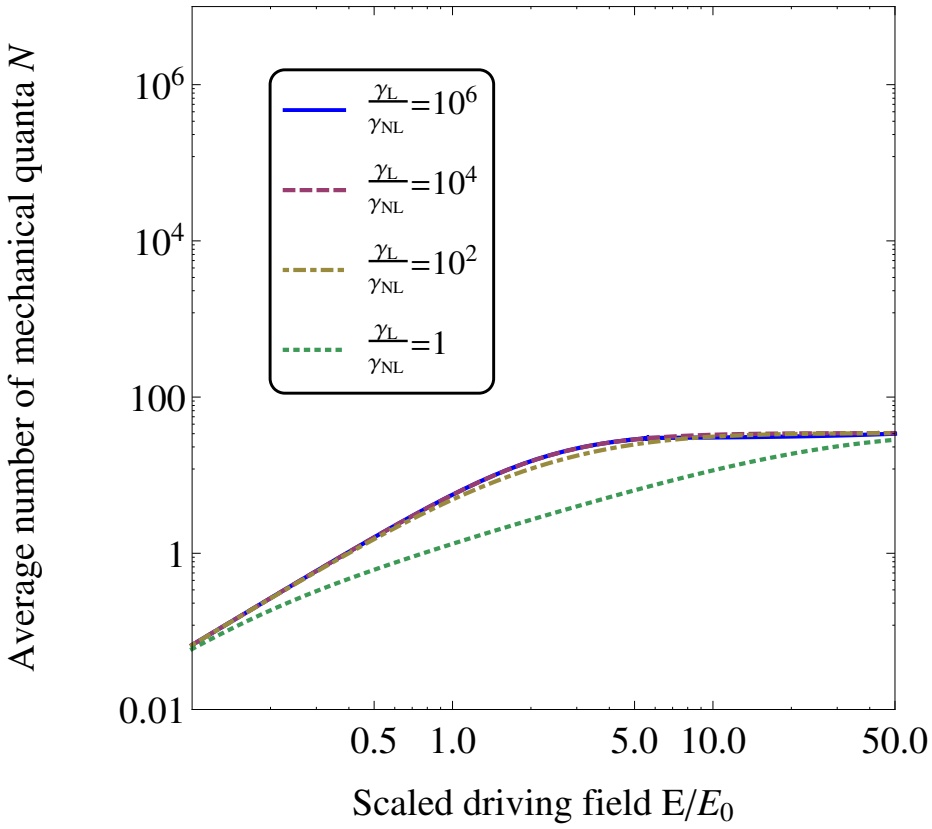

Figure 5.3: The average number of vibrational quanta $\mathcal{N}$ in the damping region, here plotted for $\Omega = \Gamma/2$. At low E, $\mathcal{N}$ increases with field strength. This is due to the raise of effective temperature of the mechanical oscillator. The increase is saturated when the dynamics is dominated by the induced electromechanical damping processes. Hence, at the saturation plateau $\mathcal{N}$ is independent of both the linear and nonlinear intrinsic damping. Here $\omega_m/\Gamma = 10^{-2}$ was used.

In the stable region at low electrical field $E < E_0$, with $E_0 = \hbar\Gamma\sqrt{\gamma_L\omega_m}/ea_0$, multi-vibron dissipation can typically be neglected due to low average occupation of mechanical quanta $\mathcal{N}$. The single-vibron processes will diffusively actuate the mechanical oscillator. The actuation can be interpreted as due to an effective temperature which is determined by the relation between the rates of increment $\Gamma_+ = \gamma_L\bar{n} + \Gamma_{+\Omega}^{+\omega_m} + \Gamma_{-\Omega}^{+\omega_m}$ and decrement $\Gamma_- = \gamma_L(\bar{n}+1) + \Gamma_{+\Omega}^{-\omega_m} + \Gamma_{-\Omega}^{-\omega_m}$ of vibrational quanta. If the driving field is strong enough the dynamics is dominated by the induced processes which then determines the effective temperature of the mechanical oscillator. At such strong field, the effective temperature, and thereby $\mathcal{N}$, saturates at a value which is independent of the intrinsic damping mechanisms, fig. 5.3.

In the pumping region, the effective temperature is increased in a similar manner as in the stable region for $E < E_0$, figs. 5.3 and 5.4. In the case of large nonlinear damping $\gamma_{NL}/\gamma_L > \omega_m/\Gamma$, the population $\mathcal{N}$ is saturated by the nonlinear processes before the instability criteria is reached, 5.4. Hence, no drastic enhancement of

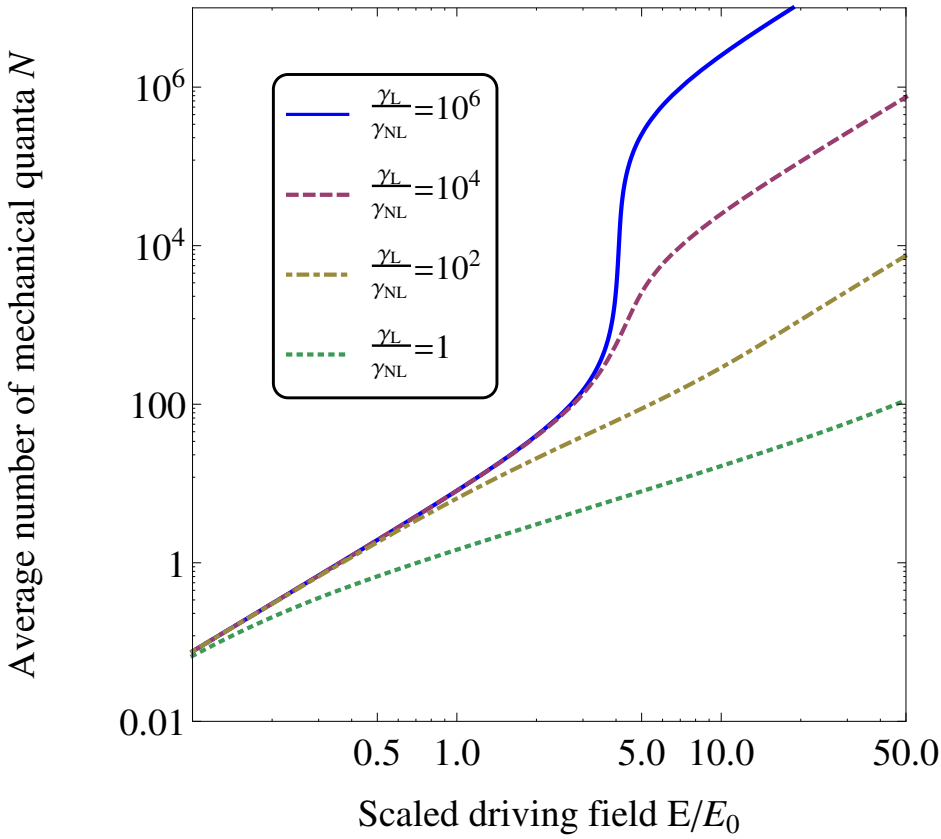

Figure 5.4: A mechanical instability may be achieved in the pumping regime, here $\Omega = 2\Gamma$. The instability manifests itself as a huge increase in $\mathcal{N}$. For large nonlinear damping (dotted) $\mathcal{N}$ is always limited by the nonlinear dissipation. Small nonlinear damping (solid) allows the effective temperature of the mechanical oscillator to increase for $E < E_0$. At $E \sim 4E_0$, the mechanics becomes unstable leading to a huge increase of the number of mechanical quanta $\mathcal{N}$. Below the instability point $\mathcal{N}$ is of the order Γ/ω_m and after the transition into the pumping region $\mathcal{N} \sim \gamma_L/\gamma_{NL}$. The width of the transition decreases with decreasing ω_m/Γ, here plotted for $\omega_m/\Gamma = 10^{-2}$.

$\mathcal{N}$ occurs. In the case of small nonlinear damping, the nonlinear effects can be neglected until the instability point is reached and $\mathcal{N}$ increases drastically to a level where it is saturated by the multi-vibron processes. Another important feature in the pumping region is that $\mathcal{N}$ is not saturated at large field strengths $E \ll E_0$ as it is in the damping region.

A final remark regards heating of the electromechanical systems caused by the absorption of energy. Since we are in the regime $\omega_m \ll \Omega$ most of the absorbed energy from the driving field will not be stored in the mechanical vibrations but in the electronic subsystem. It is assumed that this energy is effectively led away and does not affect the dynamics. It is likely that the electromechanical system to some degree will be heated. However, this might be a larger issue if one was interested in cooling and not mechanical activation of the mechanical oscillator.

5.3 Selective mode actuation in isolated oscillators

The shift of the mechanical damping for mode n of the isolated oscillator is qualitatively described by the normalised damping coefficient $\eta_n(\Omega)/n^2$, fig. 5.5. The damping coefficient of the nth mechanical mode $\eta_n(\Omega/\omega_p)$ becomes negative at a critical value $\Omega_n^{\mathrm{c}}(\tilde{\nu}) \sim \omega_p$ and reaches its minima $\eta_n^{\min}(\tilde{\nu})$ at the minima frequency $\Omega_n^{\min}(\tilde{\nu})$. If the plasma oscillation is overdamped $\tilde{\nu} = 3$, fig. 5.5(a), the characteristic width of the minima is much greater than the distance between the minima frequencies $\Omega_n^{\min}$. In the underdamped case $\tilde{\nu} = 1/3$, fig. 5.5(c), the distances between the minima frequencies become greater than the width of the minima.

If the effective pumping generated by the high-frequency external field for a given mode overcomes the intrinsic mechanical damping, the mode gets nonresonantly actuated. The actuation is due to a geometric resonance of the wave vectors of the mechanical and plasma oscillation. This allows for the actuation of both symmetric and anti-symmetric mechanical modes.

The selective nonresonant excitation of the mechanical modes is achievable for $\tilde{\nu} \ll 1$. However, there are limitations of the hydrodynamic model which limits the $\tilde{\nu}$ and n that can be considered. The hydrodynamic equations are not valid for ballistic propagation of the electrons. Introducing the effective electron mean free path $l_{\mathrm{sc}} = v_{\mathrm{F}}/\nu$ gives the relation $\tilde{\nu} = \nu/\omega_p = 0.27 l/l_{sc}\sqrt{k_{\mathrm{F}} l} \simeq 0.1 l/l_{sc}$, with Fermi wave vector k_{F}. The hydrodynamic approach fails when l_{sc} exceeds characteristic space variations in the system $l_{sc} > l/n$. Further, the semiclassical approach fails when $k_{\mathrm{F}} l < 1$.

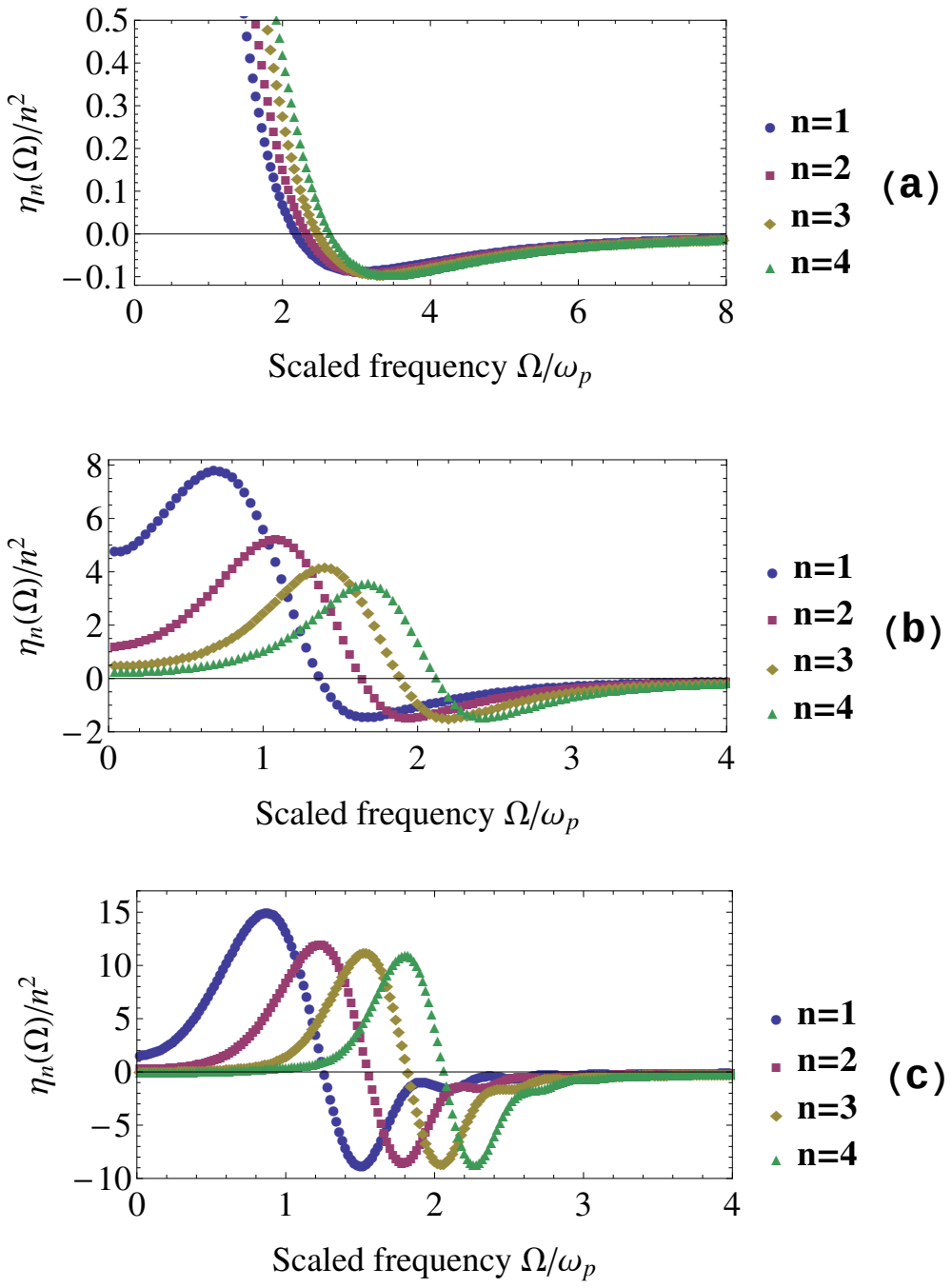

Figure 5.5: The damping coefficient $\eta_n(\Omega)/n^2$ for damping ratio ν/ω_p equal 3, 1 and 1/3 in (a), (b) and (c), respectively. The damping coefficient takes negative values slightly above $\Omega > \omega_p$. Selective actuation of mechanical modes can be achieved if $\nu < \omega_p$ due to the geometric resonance of plasma and mechanical oscillations. Here, even n indicate anti-symmetric modes and $n = 1$ denotes the fundamental mode.

Chapter 6

Conclusions and outlook

To conclude, the investigated electromechanical coupling in nano oscillators give rise to a mechanical instability of the nanoelectromechanical systems generated by a nonresonant high-frequency external electrical field. The mechanism relies on the delayed feedback between the mechanical and electronic subsystems. The phenomenon appears when the system is driven with a frequency comparable to the characteristic frequency of the charge dynamics. To reach the instability point two criteria have to be met.

Firstly, the driving frequency has to lie within the pumping region so that the net effect of the induced processes pump mechanical vibrations. Secondly, the driving field strength has to be large enough so that the induced pumping overcomes the intrinsic mechanical damping. The saturation mechanism of the unstable mechanics is proposed to be of nonlinear dissipative origin. The investigated effect is robust and not limited to specific properties of the carbon based oscillators.

The investigation of isolated suspended graphene sheets indicate that both symmetric and anti-symmetric vibrational modes can selectively be activated by a homogeneous gate-field. This is due to a geometrical resonance of the mechanical wave vector and the induced plasma wave vector.

It would be very interesting to see experimental investigations of the nonresonant instability presented in this thesis. Especially interesting would be to see if selective actuation of vibrational modes, with a homogeneous external field, can be achieved experimentally.

Extensions of the theoretical research could be to investigate

- stochastic processes in the classical description.
- anharmonic terms in the quantum mechanical model.
- nonlinear effects from the electrostatic interaction with the gate electrode.
- models going beyond the hydrodynamic description to describe semi-ballistic electrons.

Acknowledgments

My greatest gratitude goes to my supervisor Leonid Gorelik. We have spent countless hours involved in discussion, always with the aim of better understanding the, to us, most interesting parts of physics. Without Leonid little of the work presented in this thesis would have been more than incomplete thoughts and vague ideas.

Further, I would like to thank my colleagues, who have tiptoed around in the corridors and made the journey both easier and much more fun. Many of you have been very helpful in times of need. Special thanks goes to the father, sister and holy spirit for proofreading my thesis and coming with valuable comments.

Finally, I would like to thank my friends and family for the support and that you take care of me when my colleagues are not on duty. Now when the thesis is written, I will stretch out my posture and come back to you.

Appendix A

Direct resonance

The direct resonance [31] is the result of a forced oscillator commonly used to actuate nanoelectromechanical oscillators [5]. It is qualitatively captured by the simple equation

$$\ddot{X} + \gamma\dot{X} + \omega_{\mathrm{m}}^2 X = \mathcal{K}\cos(\omega t), \tag{A.1}$$

with frequency $\omega = 2\Omega$ and driving strength $\mathcal{K} = C_G(0)V_G^2/4md^2$ to correspond to eq. (2.12). Let us disregard the transient processes of the initial conditions. An approximate solution to this equation can be found on the form

$$X(t) = a(\omega)\cos(\omega t - \phi), \tag{A.2}$$

$$a(\Omega) = \frac{\mathcal{K}}{\Delta}, \quad \phi = \arccos\left(\frac{\omega_{\mathrm{m}}^2 - \omega^2}{\Delta}\right), \quad \Delta = \sqrt{(\omega_{\mathrm{m}}^2 - \omega^2)^2 + \gamma^2\omega^2} \tag{A.3}$$

i.e., a phase shifted response with the same frequency as the driving field. If the oscillator starts at a relatively small amplitude, this driving force will lead to a linear time growth of the amplitude $a(\Omega)$. The stationary amplitude exhibits a Lorentzian curve with characteristic width γ and maximum at the resonance condition $\omega \approx \omega_{\mathrm{m}}$ for a resonator with high quality factor $Q \gg 1$. As the frequency mismatch between the driving field and the resonator $\Omega - \omega_{\mathrm{m}}$ increases the amplitude of the actuated oscillation diminishes.

Appendix B

Parametric instability

The other resonance phenomenon is the parametric instability [31] which is present in some nanoelectromechanical systems [16]. It is qualitatively described by the equation

$$\ddot{X} + \gamma\dot{X} + \omega_{\mathrm{m}}^2 X = \mathcal{K} X \cos(\omega t), \tag{B.1}$$

known as the *Mathieu's equation* in the case of $\gamma = 0$. This type of driving can be viewed as a modulation of the oscillator frequency $\omega^2 = \omega_{\mathrm{m}}^2 - \mathcal{K}\cos(\omega t)$. Let us assume the modulation to be small $\mathcal{K}/\omega_{\mathrm{m}}^2 \ll 1$ and seek a solution with the Ansatz

$$X(t) = a(t)\cos(\omega t/2) + b(t)\sin(\omega t/2), \tag{B.2}$$

where $a(t)$ and $b(t)$ varies slowly in time in comparison with the trigonometrical factors. This solution will only be perturbatively correct since X will also include terms with all frequencies $n\Omega/2$ where n runs over all positive integers. The stationary state $X = 0$ becomes unstable under the following conditions

$$-\sqrt{\left(\frac{\mathcal{K}}{2\omega_{\mathrm{m}}}\right)^2 - \gamma^2} < \omega - 2\omega_{\mathrm{m}} < \sqrt{\left(\frac{\mathcal{K}}{2\omega_{\mathrm{m}}}\right)^2 - \gamma^2}. \tag{B.3}$$

The instability is only possible if the driving field is strong enough so that the induced pumping overcomes the intrinsic mechanical damping $\mathcal{K}/\omega_{\mathrm{m}} > 2\gamma$. Further, the detuning from the resonance condition $\omega = 2\omega_{\mathrm{m}}$ has to lie within the frequency window eq. (B.3) in which the mechanical motion is unstable. In the unstable region the amplitude of oscillations will grow exponentially with the rate $\nu = \sqrt{(\mathcal{K}/2\omega_{\mathrm{m}})^2 - (\omega - 2\omega_{\mathrm{m}})^2} - \gamma$. Parametric instabilities are also achieved at driving frequencies meeting the resonance conditions $\omega = 2\omega_{\mathrm{m}}/n$. However, the corresponding threshold for the driving strength $\mathcal{K}$ is increased and proportional to $\gamma^{1/n}$.

Appendix C

Tracing over electronic subsystem

In this appendix, a derivation of the rate equation which governs the dynamics of the stationary average vibrational quanta is presented. Let us assume the electronic subsystem to be in thermal equilibrium with the non-interacting Hamiltonian at temperature T,

$$\hat{\rho}_{\mathrm{eq}} = Z^{-1} \exp\left(- \int \mathrm{d}\varepsilon \nu_\varepsilon \hat{\psi}_\varepsilon^\dagger \hat{\psi}_\varepsilon / k_{\mathrm{B}} T \right) \tag{C.1}$$

where

$$Z = \mathrm{tr}\left[\exp\left(- \int \mathrm{d}\varepsilon \nu_\varepsilon \hat{\psi}_\varepsilon^\dagger \hat{\psi}_\varepsilon / k_{\mathrm{B}} T \right) \right] \tag{C.2}$$

is the partition function. For a more convenient notation we introduce $\hat{H}_{\mathrm{int}} = \hat{H}_{\mathrm{i}}(e^{i\Omega t} + e^{-i\Omega t})$ where $\hat{H}_{\mathrm{i}} = eEa_0(\hat{c}^\dagger + \hat{c})\hat{d}^\dagger \hat{d}$. We start from the quantum Liouville equation which describes the time evolution of the total density operator $\hat{\rho}$,

$$i\hbar \frac{\partial}{\partial t} \hat{\rho} = \left[\hat{H}_0 + \left(e^{i\Omega t} + e^{-i\Omega t} \right) \hat{H}_{\mathrm{i}}, \hat{\rho} \right]. \tag{C.3}$$

Let us assume the electronic subsystem to always be in its equilibrium distribution due to fast relaxation processes not governed by eq. (C.3). The density operator can then be separated into the form $\hat{\rho}(t) = \hat{\rho}_{\mathrm{m}}(t) \otimes \hat{\rho}_{\mathrm{eq}}$, where $\hat{\rho}_{\mathrm{m}}(t)$ is the density operator of the mechanical subsystem and the electronic subsystem fulfiles $\left[\hat{H}_0, \hat{\rho}_{\mathrm{eq}}\right] = 0$. We expand the mechanical density operator $\hat{\rho}_{\mathrm{m}}(t) = \sum_{n=-\infty}^{\infty} \hat{\rho}_n \exp(in\Omega t)$ where $\hat{\rho}_n = \sum_{k=0}^{\infty} \hat{\rho}_n^{(k)}$ and $\hat{\rho}_n^{(k)} \propto \varepsilon^{|n|+2k}$ with the small parameter $\varepsilon = eEa_0/(2\hbar\Omega) \ll 1$. This gives an infinite set of coupled equations, one for each frequency $n\Omega$.

To continue the analysis we have to perform some sort of approximation. We choose to truncate the coupled dynamics at order ε^2 which results in the closed set of equations

$$0 = \left[\hat{H}_{\mathrm{i}}, \hat{\rho}_{+1}^{(0)} \otimes \hat{\rho}_{\mathrm{eq}} \right] + \left[\hat{H}_{\mathrm{i}}, \hat{\rho}_{-1}^{(0)} \otimes \hat{\rho}_{\mathrm{eq}} \right] \tag{C.4}$$

$$\mp \hbar\Omega \hat{\rho}_{\pm 1}^{(0)} \otimes \hat{\rho}_{\mathrm{eq}} = \left[\hat{H}_0, \hat{\rho}_{\pm 1}^{(0)} \otimes \hat{\rho}_{\mathrm{eq}} \right] + \left[\hat{H}_{\mathrm{i}}, \hat{\rho}_0^{(0)} \otimes \hat{\rho}_{\mathrm{eq}} \right] \tag{C.5}$$

where we have assumed the stationary term $\hat{\rho}_0^{(0)}$ and $\hat{\rho}_0^{(1)}$ to be diagonal in the $|n\rangle$ basis due to dephasing processes not governed by (C.3). Using the residue theorem

we can express the operators

$$\hat{\rho}^{(0)}_{\pm 1} \otimes \hat{\rho}_{\mathrm{eq}} = -\frac{1}{2\pi i} \int \mathrm{d}\varepsilon \; \hat{G}_+(\varepsilon \mp \hbar\Omega) \left[\hat{H}_{\mathrm{i}}, \hat{\rho}^{(0)}_0 \otimes \hat{\rho}_{\mathrm{eq}} \right] \hat{G}_-(\varepsilon), \quad \hat{G}_\pm(x) = \frac{1}{\hat{H}_0 - x \pm i\delta}, \tag{C.6}$$

where $\delta \to 0$ and $\hat{G}_+(x)$ $\left(\hat{G}_-(x)\right)$ has a pole in the upper (lower) complex plane and fulfilles the identity

$$\delta(\hat{H}_0 - x) = 2\pi i \left(\hat{G}_-(x) - \hat{G}_+(x) \right). \tag{C.7}$$

We substitute this expression for $\hat{\rho}^{(0)}_{\pm} \otimes \hat{\rho}_{\mathrm{eq}}$ into eq. (C.4) and obtain an equation for the stationary density operator $\hat{\rho}^{(0)}_0 \otimes \hat{\rho}_{\mathrm{eq}}$. Eq. (C.4) contains eight terms due to the two nested commutator terms. Two of these terms, one from each nested commutator are

$$\begin{aligned} \chi = -\frac{1}{2\pi i} \int \mathrm{d}\varepsilon \; \Big(& \hat{H}_{\mathrm{i}} \hat{G}_-(\varepsilon + \hbar\Omega) \hat{H}_{\mathrm{i}} \hat{\rho}^{(0)}_0 \otimes \hat{\rho}_{\mathrm{eq}} \hat{G}_+(\varepsilon) + \\ & \hat{\rho}^{(0)}_0 \otimes \hat{\rho}_{\mathrm{eq}} \hat{G}_-(\varepsilon - \hbar\Omega) \hat{H}_{\mathrm{i}} \hat{G}_+(\varepsilon) \hat{H}_{\mathrm{i}} \Big). \end{aligned} \tag{C.8}$$

We shift the argument of the last term $\varepsilon - \hbar\Omega \to \varepsilon$. One of the $\hat{G}$-operators in each term can be substituted by a Dirac delta-function according to eq. (C.7). This is since the integral along the real axis, with poles only in the upper or the lower complex plane, is zero. We then have

$$\begin{aligned} \chi = \int \mathrm{d}\varepsilon \; \Big(& \hat{H}_{\mathrm{i}} \hat{G}_-(\varepsilon + \hbar\Omega) \hat{H}_{\mathrm{i}} \hat{\rho}^{(0)}_0 \otimes \hat{\rho}_{\mathrm{eq}} \delta(\varepsilon - \hat{H}_0) - \\ & \hat{\rho}^{(0)}_0 \otimes \hat{\rho}_{\mathrm{eq}} \delta(\varepsilon - \hat{H}_0) \hat{H}_{\mathrm{i}} \hat{G}_+(\varepsilon + \hbar\Omega) \hat{H}_{\mathrm{i}} \Big). \end{aligned} \tag{C.9}$$

Since our aim is to trace over the electronic states we may cycle $\hat{\rho}^{(0)}_0$ and the delta functions. Combining the remaining $\hat{G}$-operators to delta functions and using the integral representation

$$\delta(\omega) = \frac{1}{2\pi} \int_{-\infty}^{\infty} \mathrm{d}t e^{-i\omega x} \tag{C.10}$$

we may write

$$\chi = i \int_{-\infty}^{\infty} \mathrm{d}t \; e^{it\Omega} e^{it\hat{H}_0/\hbar} \hat{H}_{\mathrm{i}} e^{-it\hat{H}_0/\hbar} \hat{H}_{\mathrm{i}} \hat{\rho}^{(0)}_0 \otimes \hat{\rho}_{\mathrm{eq}} \tag{C.11}$$

Calculating the interaction picture of the first interaction Hamiltonian and substituting all operators give

$$\begin{aligned} \chi = & \left(\frac{eEa_0}{2} \right)^2 \int_{-\infty}^{\infty} \mathrm{d}t \int_{-\infty}^{\infty} \mathrm{d}\varepsilon_1 \mathrm{d}\varepsilon_2 \mathrm{d}\varepsilon_3 \mathrm{d}\varepsilon_4 \; b(\varepsilon_1) b^*(\varepsilon_2) b(\varepsilon_3) b^*(\varepsilon_4) \times \\ & e^{i\Omega t} \left(\hat{c}^\dagger e^{i\omega_{\mathrm{m}} t} + \hat{c} e^{-i\omega_{\mathrm{m}} t} \right) \left(\hat{c}^\dagger + \hat{c} \right) e^{i(\varepsilon_1 - \varepsilon_2)t/\hbar} \hat{\psi}^\dagger_{\varepsilon_1} \hat{\psi}_{\varepsilon_2} \hat{\psi}^\dagger_{\varepsilon_3} \hat{\psi}_{\varepsilon_4} \hat{\rho}^{(0)}_0 \otimes \hat{\rho}_{\mathrm{eq}} \end{aligned} \tag{C.12}$$

The trace can be calculated by using the commutation relations for the fermionic operators and successively moving one operator around one whole cycle. The result is

$$\mathrm{tr}\left(\hat{\psi}^{\dagger}_{\varepsilon_1}\hat{\psi}_{\varepsilon_2}\hat{\psi}^{\dagger}_{\varepsilon_3}\hat{\psi}_{\varepsilon_4}\hat{\rho}_{\mathrm{eq}}\right) = \delta\Big(\nu(\varepsilon_1-\varepsilon_2)\Big)\delta\Big(\nu(\varepsilon_3-\varepsilon_4)\Big)n_{\mathrm{f}}(\varepsilon_1)n_{\mathrm{f}}(\varepsilon_2) + \\ \delta(\nu\Big(\varepsilon_1-\varepsilon_4)\Big)\delta\Big(\nu(\varepsilon_2-\varepsilon_3)\Big)n_{\mathrm{f}}(\varepsilon_1)\Big(1-n_{\mathrm{f}}(\varepsilon_3)\Big). \quad \text{(C.13)}$$

Two of the integrals over ε_i in eq. (C.12) takes out the delta functions in eq. (C.13) and the integral over t gives a delta function for energy conservation. The contribution from the other six terms in eq. (C.4) can be calculated in an analogous manner. Since $\hat{\rho}_0^{(0)}$ is diagonal in the ladder basis we can omit off-diagonal terms and arrive at the rate equation of the stationary density operator

$$\Gamma^{-}\left(\hat{c}\hat{\rho}_{\mathrm{st}}\hat{c}^{\dagger} - \hat{c}^{\dagger}\hat{c}\hat{\rho}_{\mathrm{st}}\right) + \Gamma^{+}\left(\hat{c}^{\dagger}\hat{\rho}_{\mathrm{st}}\hat{c} - \hat{c}\hat{c}^{\dagger}\hat{\rho}_{\mathrm{st}}\right) = 0 \quad \text{(C.14)}$$

with $\Gamma^{\pm} = \Gamma^{\pm\omega_{\mathrm{m}}}_{+\Omega} + \Gamma^{\pm\omega_{\mathrm{m}}}_{-\Omega}$ and

$$\Gamma^{\pm\omega_{\mathrm{m}}}_{\pm\Omega} = \frac{(eEa_0)^2}{2\pi\hbar^2\Gamma}\int \mathrm{d}\varepsilon_1\mathrm{d}\varepsilon_2 n_{\mathrm{f}}(\varepsilon_1)\Big(1-n_{\mathrm{f}}(\varepsilon_2)\Big)\frac{(\hbar\Gamma)^3\delta(\varepsilon_2-\varepsilon_1\pm\hbar\Omega\pm\hbar\omega_{\mathrm{m}})}{|\varepsilon_1-\varepsilon_0+i\hbar\Gamma|^2\,|\varepsilon_2-\varepsilon_0+i\hbar\Gamma|^2}. \quad \text{(C.15)}$$

By comparing this with the linear Lindblad superoperator in eq (4.10), it is evident that they have the same structure under the diagonal condition of $\hat{\rho}$. We add the dissipative superoperator terms at zero temperature to eq. (C.14). By projecting eq. (C.14) on the diagonal state $\langle n|...|n\rangle$ we get the difference equation

$$\gamma_{\mathrm{NL}}(n+1)(n+2)P_{n+2} + (\Gamma^{-}+\gamma_{\mathrm{L}})(n+1)P_{n+1} + \Gamma^{+}nP_{n-1} \\ -\left(\gamma_{\mathrm{NL}}n(n-1) + (\Gamma^{-}+\gamma_{\mathrm{L}})n + \Gamma^{+}(n+1)\right)P_n = 0. \quad \text{(C.16)}$$

for the stationary occupation probabilities $P_n = \langle n|\hat{\rho}_0^{(0)}|n\rangle$.

Appendix D

Rate equation of mechanical quanta

The aim of this appendix is to find an expression for the stationary average number of vibrational quanta $\mathcal{N}$ governed by the rate equation derived in Appendix C,

$$\begin{aligned}\gamma_{\mathrm{NL}}(n+1)(n+2)P_{n+2}+(\Gamma^{-}+\gamma_{\mathrm{L}})(n+1)P_{n+1}+\Gamma^{+}nP_{n-1}\\ -\left(\gamma_{\mathrm{NL}}n(n-1)+(\Gamma^{-}+\gamma_{\mathrm{L}})n+\Gamma^{+}(n+1)\right)P_n=0.\end{aligned} \tag{D.1}$$

Let us introduce $\mathcal{P}(z)=\sum_{n=0}^{\infty}z^nP_n$ where z is a complex number inside the unit circle. The probabilities P_n have to sum up to 1 which gives $\mathcal{P}(1)=1$ and $\mathcal{P}(-1)$ has to be absolute convergent. The trick is to multiply eq. (D.1) by z^n and sum over $\sum_{n=0}^{\infty}$. The first term in eq. (D.1) can then be manipulated

$$\sum_{n=0}^{\infty}z^n(n+1)(n+2)P_{n+2}=\frac{\partial^2}{\partial z^2}\sum_{n=0}^{\infty}z^{n+2}P_{n+2}=\frac{\partial^2}{\partial z^2}(\mathcal{P}(z)-P_0-zP_1)=\frac{\partial^2}{\partial z^2}\mathcal{P}(z). \tag{D.2}$$

Similarly term three in eq. (D.1) can then be manipulated by using $P_{-1}=0$, no probability to occupy 'negative' numbers of vibrational quanta,

$$\begin{aligned}\sum_{n=0}^{\infty}z^nnP_{n-1}=\sum_{m=0}^{\infty}z^{m+1}(m+1)P_m=z\frac{\partial}{\partial z}\sum_{m=0}^{\infty}z^{m+1}P_m=z\frac{\partial}{\partial z}\Big(z\mathcal{P}(z)\Big)=\\ z\left(1+z\frac{\partial}{\partial z}\right)\mathcal{P}(z).\end{aligned} \tag{D.3}$$

The other terms can be manipulated in an analogous manner. Summing all terms in eq. (C.16) and excluding the common factor of $1-z$ result in the homogeneous second order differential equation

$$(1+z)\frac{\partial^2}{\partial z^2}\mathcal{P}(z)+\frac{\Gamma^{-}+\gamma_{\mathrm{L}}}{\gamma_{\mathrm{NL}}}\frac{\partial}{\partial z}\mathcal{P}(z)-\frac{\Gamma^{+}}{\gamma_{\mathrm{NL}}}\left(1+z\frac{\partial}{\partial z}\right)\mathcal{P}(z)=0. \tag{D.4}$$

Generally, a second order differential equation with non-constant terms cannot be solved. However, rewriting the second order and last term of eq. (D.4) gives

$$\frac{\partial}{\partial z}\left((1+z)\frac{\partial}{\partial z}\mathcal{P}(z)\right)-\frac{\partial}{\partial z}\mathcal{P}(z)+\frac{\Gamma^{-}+\gamma_{\mathrm{L}}}{\gamma_{\mathrm{NL}}}\frac{\partial}{\partial z}\mathcal{P}(z)-\frac{\Gamma^{+}}{\gamma_{\mathrm{NL}}}\frac{\partial}{\partial z}\Big(z\mathcal{P}(z)\Big)=0. \tag{D.5}$$

This equation can be integrated trivially in z yielding a non-homogeneous first order differential equation

$$\frac{\partial}{\partial z}\mathcal{P}(z) - h(z)\mathcal{P}(z) = g(z), \quad h(z) = \frac{\left(1 - \frac{\Gamma^- + \gamma_L}{\gamma_{NL}} + \frac{\Gamma^+}{\gamma_{NL}} z\right)}{1+z}, \quad g(z) = \frac{C_1}{1+z} \tag{D.6}$$

where C_i, $i = 1, 2...$ are constants of integration. The homogeneous solution $\mathcal{P}_h(z) = \exp(f(z))$ where $f'(z) = h(z)$. The particular solution can be written as $\mathcal{P}_p(z) = \int_{-1}^{z} dz' \exp(f(z) - f(z'))g(z')$. With $f(z) = (1 - (\Gamma^+ + \Gamma^- + \gamma_L)/\gamma_{NL})\ln(1+z) + (1+z)\Gamma^+/\gamma_{NL} + C_2$ the full solution takes the form

$$\mathcal{P}(z) = C_3(1+z)^{\left(1 - \frac{\Gamma^+ + \Gamma^- + \gamma_L}{\gamma_{NL}}\right)} + C_4 \int_{-1}^{z} dz' \left(\frac{1+z'}{1+z}\right)^{\left(\frac{\Gamma^+ + \Gamma^- + \gamma_L}{\gamma_{NL}} - 1\right)} \frac{e^{\frac{\Gamma^+}{\gamma_{NL}}(z-z')}}{1+z'}. \tag{D.7}$$

To satisfy the absolute convergence criteria at $z = -1$ of $\mathcal{P}(z)$ the constant C_3 has to be zero. We integrate by parts to obtain a more transparent solution

$$\mathcal{P}(z) = C\left(1 + \frac{\Gamma^+}{\gamma_{NL}} \int_{-1}^{z} dz' \left(\frac{1+z'}{1+z}\right)^{\left(\frac{\Gamma^+ + \Gamma^- + \gamma_L}{\gamma_{NL}} - 1\right)} e^{\frac{\Gamma^+}{\gamma_{NL}}(z-z')}\right) \tag{D.8}$$

where the constant is given by the condition $\mathcal{P}(1) = 1$,

$$C = \left(1 + \frac{\Gamma^+}{\gamma_{NL}} \int_{-1}^{z} dz' \left(\frac{1+z'}{1+z}\right)^{\left(\frac{\Gamma^+ + \Gamma^- + \gamma_L}{\gamma_{NL}} - 1\right)} e^{\frac{\Gamma^+}{\gamma_{NL}}(z-z')}\right)^{-1}. \tag{D.9}$$

The stationary average number of vibrational quanta $\mathcal{N}$ is then given by the relation $\mathcal{N} = \partial_z \mathcal{P}(z)$.

Bibliography

[1] A. K. Geim and K. S. Novoselov. The rise of graphene. *Nature Materials*, 6(3):183–191, 2007.

[2] K. S. Novoselov, V. I. Fal'ko, L. Colombo, P. R. Gellert, M. G. Schwab, and K. Kim. A roadmap for graphene. *Nature*, 490:192–200, 2012.

[3] M. Terrones, A. R. Botello-Méndez, J. Campos-Delgado, F. López-Urías, Y. I. Vega-Cantú, F. J. Rodríguez-Macías, A. L. Elas, E. Muñoz-Sandoval, A. G. Cano-Márquez, J. Charlier, and H. Terrones. Graphene and graphite nanoribbons: Morphology, properties, synthesis, defects and applications. *Nano Today*, 5(4):351 – 372, 2010.

[4] C. Lee, X. Wei, J. W. Kysar, and J. Hone. Measurement of the elastic properties and intrinsic strength of monolayer graphene. *Science*, 321(5887):385–388, 2008.

[5] B. Lassagne, Y. Tarakanov, J. Kinaret, D. Garcia-Sanchez, and A. Bachtold. Coupling mechanics to charge transport in carbon nanotube mechanical resonators. *Science*, 325(5944):1107–1110, 2009.

[6] R. Bogue. Graphene sensors: a review of recent developments. *Sensor Review*, 34(3):233–238, 2014.

[7] J. Chaste, A. Eichler, J. Moser, G. Ceballos, R. Rurali, and A. Bachtold. A nanomechanical mass sensor with yoctogram resolution. *Nat. Nano.*, 7(5):301–304, 2012.

[8] C. Chen, S. Rosenblatt, K. I. Bolotin, W. Kalb, P. Kim, I. Kymissis, H. L. Stormer, T. F. Heinz, and J. Hone. Performance of monolayer graphene nanomechanical resonators with electrical readout. *Nature Nanotechnology*, 4(12):861–867, 2009.

[9] H. B. Meerwaldt, G. Labadze, B. H. Schneider, A. Taspinar, Ya. M. Blanter, H. S. J. van der Zant, and G. A. Steele. Probing the charge of a quantum dot with a nanomechanical resonator. *Phys. Rev. B*, 86:115454, Sep 2012.

[10] J. Moser, J. Guttinger, A. Eichler, M. J. Esplandiu, D. E. Liu, M. I. Dykman, and A. Bachtold. Ultrasensitive force detection with a nanotube mechanical resonator. *Nat. Nano.*, 8(7):493–496, 2013.

[11] J. Atalaya, A. Isacsson, and M. I. Dykman. Diffusion-induced bistability of driven nanomechanical resonators. *Phys. Rev. Lett.*, 106:227202, May 2011.

[12] C. Chen, S. Lee, V. V. Deshpande, G. Lee, M. Lekas, K. Shepard, and J. Hone. Graphene mechanical oscillators with tunable frequency. *Nature Nanotechnology*, 8:923–927, 2013.

[13] Y. Xu, C. Chen, V. V. Deshpande, F. A. DiRenno, A. Gondarenko, D. B. Heinz, S. Liu, P. Kim, and J. Hone. Radio frequency electrical transduction of graphene mechanical resonators. *Applied Physics Letters*, 97(24):243111, 2010.

[14] D. Garcia-Sanchez, A. M. van der Zande, A. S. Paulo, B. Lassagne, P. L. McEuen, and A. Bachtold. Imaging mechanical vibrations in suspended graphene sheets. *Nano Letters*, 8(5):1399–1403, 2008.

[15] M. Poot, S. Etaki, I. Mahboob, K. Onomitsu, H. Yamaguchi, Ya. M. Blanter, and H. S. J. van der Zant. Tunable backaction of a dc squid on an integrated micromechanical resonator. *Phys. Rev. Lett.*, 105:207203, Nov 2010.

[16] Q. P. Unterreithmeier, E. M. Weig, and J. P. Kotthaus. Universal transduction scheme for nanomechanical systems based on dielectric forces. *Nature*, 458(7241):1001–1004, 2009.

[17] L. Y. Gorelik, A. Isacsson, M. V. Voinova, B. Kasemo, R. I. Shekhter, and M. Jonson. Shuttle mechanism for charge transfer in coulomb blockade nanostructures. *Phys. Rev. Lett.*, 80(cond-mat/9711196. APR-97-75. 20):4526–4529, 1998.

[18] A. Isacsson, L. Y. Gorelik, M. V. Voinova, B. Kasemo, R. I. Shekhter, and M. Jonson. Shuttle instability in self-assembled coulomb blockade nanostructures. *Physica B: Condensed Matter*, 255(1-4):150–163, 1998.

[19] C. H. Metzger and K. Karrai. *Nature*, 432:1002–1005, Dec 2004.

[20] T. J. Kippenberg and K. J. Vahala. Cavity optomechanics: Back-action at the mesoscale. *Science*, 321(5893):1172–1176, 2008.

[21] R. A. Barton, Isaac R. Storch, V. P. Adiga, R. Sakakibara, B. R. Cipriany, B. Ilic, S. P. Wang, P. Ong, P. L. McEuen, J. M. Parpia, and H. G. Craighead. Photothermal self-oscillation and laser cooling of graphene optomechanical systems. *Nano Letters*, 12(9):4681–4686, 2012. PMID: 22889415.

[22] Tero T. Heikkilä. *Physics of Nanoelectronics: Transport and Fluctuation Phenomena at Low Temperatures*. OUP Oxford Master Series in Physics, Oxford GBR, 2014. pp. 218-219.

[23] K. Brown, J. Britton, R. Epstein, J. Chiaverini, D. Leibfried, and D. Wineland. Passive cooling of a micromechanical oscillator with a resonant electric circuit. *Phys. Rev. Lett.*, 99:137205, Sep 2007.

[24] M. Bagheri, M. Poot, M. Li, W. P. H. Pernice, and H. X. Tang. Dynamic manipulation of nanomechanical resonators in the high-amplitude regime and non-volatile mechanical memory operation. *Nature Nanotechnology*, 6(11):726–732, 2011.

[25] J. Xia, F. Chen, J. Li, and N. Tao. Measurement of the quantum capacitance of graphene. *Nature Nanotechnology*, 4(8):504–509, 2009.

[26] A. M. Eriksson, D. Midtvedt, A. Croy, and A. Isacsson. Frequency tuning, nonlinearities and mode coupling in circular mechanical graphene resonators. *Nanotechnology*, 24(39):395702, 2013.

[27] K. N. Kudin, G. E. Scuseria, and B. I. Yakobson. c_2F, bn, and c nanoshell elasticity from *ab initio* computations. *Phys. Rev. B*, 64:235406, Nov 2001.

[28] S. Y. Kim and H. S. Park. The importance of edge effects on the intrinsic loss mechanisms of graphene nanoresonators. *Nano Letters*, 9(3):969–974, 2009. PMID: 19239202.

[29] A. H. Nayfeh and D. T. Mook. *Nonlinear Oscillations*. WILEY-VCH Verlag & GmbH Co. KGaA, 2004.

[30] L. D. Landau, E. M. Lifshitz, and L. P. Pitaevskii. *Electrodynamics of Continuous Media vol. 8 of Course of Theoretical Physics*. Butterworth-Heinemann, Oxford, 1984. 2nd edition, pp. 29-30.

[31] L. D. Landau and E. M. Lifshitz. *Mechanics vol. 1 of course of theoretical physics*. Pergamon Press Ltd., Oxford, 1976. 3rd edition, pp. 80-83.

[32] A. Eichler, J. Moser, J. Chaste, M. Zdrojek, I. Wilson-Rae, and A. Bachtold. Nonlinear damping in mechanical resonators made from carbon nanotubes and graphene. *Nat. Nanotechnol.*, 6:339–342, 2011.

[33] A. Croy, D. Midtvedt, A. Isacsson, and J. M. Kinaret. Nonlinear damping in graphene resonators. *Phys. Rev. B*, 86:235435, 2012.

[34] M. Jablan, M. Soljacic, and H. Buljan. Plasmons in graphene: Fundamental properties and potential applications. *Proceedings of the IEEE*, 101(7):1689–1704, July 2013.

[35] H. Carmichael. *An Open Systems Approach to Quantum Optics*. Springer Verlag, 1991. pp. 6-9.

[36] A. Voje, A. Croy, and A. Isacsson. Multi-phonon relaxation and generation of quantum states in a nonlinear mechanical oscillator. *New Journal of Physics*, 15(5):053041, 2013.